ZERO FIELD LEVEL CROSSING

IN THE HELIUM ATOM

by

ROBERT ECKARDT BARDSLEY

B.Sc., University of British Columbia, 1968

A THESIS SUBMITTED IN PARTIAL FULFILLMENT OF

THE REQUIREMENTS FOR THE DEGREE OF

MASTER OF SCIENCE

in the Department

of

PHYSICS

----We accept this thesis as conforming to the
required standard

THE UNIVERSITY OF BRITISH COLUMBIA

September, 1970

ABSTRACT

Zero-field level crossing techniques have been used to measure some upper state lifetimes of the helium atom. The upper states of the atom were excited in a discharge between two capacitor plates. A radio frequency voltage was applied to these plates by a 450 MHz source. The emitted light was modulated by rotating a quarter-wave plate in front of a polaroid in the beam of emitted light. The polarization, which is directly related to this modulation, was measured by a phase sensitive lock-in amplifier.

The halfwidths of curves obtained by plotting the polarization against the magnetic field strength for the n^1D - 2^1P transitions yielded lifetimes of; 2.71×10^{-8} sec. for the 3^1D state, 3.97×10^{-8} sec. for the 4^1D state and 4.48×10^{-8} sec. for the 5^1D state.

TABLE OF CONTENTS

TABLE OF CONTENTS (cont'd.)

LIST OF TABLES

ILLUSTRATIONS AND FIGURES

ILLUSTRATIONS AND FIGURES (cont'd.)

ACKNOWLEDGEMENTS

I wish to express my sincere appreciation to Professor F. W. Dalby for his encouragement and his guidance. I am particularly thankful for his ceaseless enthusiasm for this project.

I am indebted to Dr. Jacob Vanderlinde for designing the apparatus and for patiently describing its operation.

The efficient typing of the thesis by Mrs. Sherri MacRaild is greatly appreciated.

Also, I thank my wife and my fellow graduate students for their worthy assistance.

CHAPTER I

INTRODUCTION

1.1 Introduction

The lifetimes of states in atoms and molecules, or the transition probability between these states have been, for many years, a difficult property to measure. In the past, elaborate methods have been used which involve interconnected systems which have properties which are difficult to measure accurately. In my opinion, the difficulty in measuring these properties or lack of knowledge of these properties produces unreliable results. For example, the Hook method involves an accurate measurement of the partial pressure of the absorbing gas. In the following experiment the lifetimes have been measured by the Hanle effect. This is a straight-forward method that involves measuring only the polarization of the emitted light as a function of the magnetic field strength.

Basically, the Hanle effect measures the natural width of a spectral line with a resolution of the order of 10^{-5} A. This will seem incredible when one considers today's spectrographs and monochromators which have a resolution of about 10^{-2} A.

Consider two Zeeman levels split by a magnetic field as shown in Fig. 1. Notice that they are completely resolved at a large magnetic field, (case 1). As the magnetic field decreases, the levels come closer together and the two levels can interfere with each other other, (case 2). By measuring the degree of interference as a function of the magnetic field, the width of the energy levels can be calculated. (This

interference will later be shown to be related to the polarization of emitted light.) The interference effects, mentioned above, are similar to the interference effects of a double slit diffraction pattern. In the double slit experiment one cannot distinguish which slit a certain photon came through. Similarly in our experiment, when the two states of the atom overlap, one cannot distinguish what state the atom was in.

The Hanle effect has been used in the past to measure lifetimes of atoms. But, its use was limited mainly to transitions excited by absorption of resonance radiation. In the present experiment, electron excitation is used. Now, one would expect that the selection of molecular states or atomic states that one can measure, is almost unlimited.
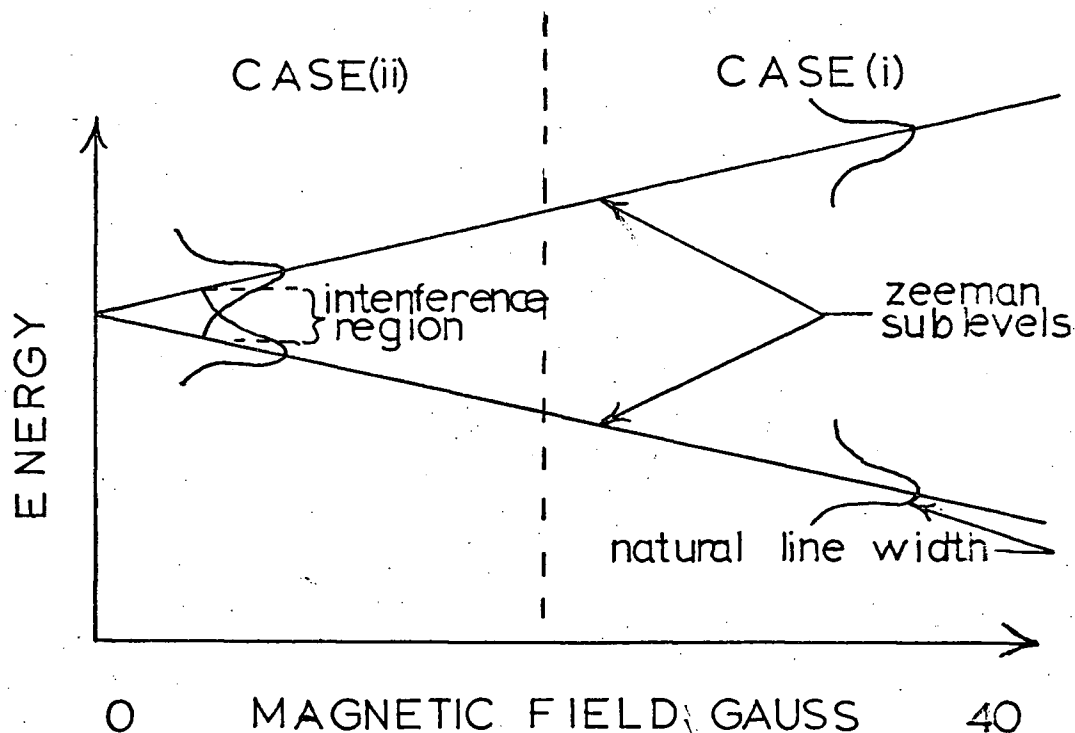
FIG. 1--Splitting of Zeeman Sublevels

Specifically, the lifetimes of the 3^1D, 4^1D, and 5^1D energy levels of the helium atom have been measured. These lifetimes are known relatively accurately, thus, the validity of the use of electron excitation to observe Hanle effect signals is substantiated.

CHAPTER II

THEORY

.2.1   Introduction

There is a classical and a quantum mechanical treatment of the
theory. The classical treatment, I feel, is beneficial to the experi-
menter in visualizing what is taking place at the time of the experiment.
The quantum treatment can be used to obtain a theoretical value for
polarization. During the discussion of the quantum theory a description
of the excitation mechanism will be given. Following this there will
be a short description of the mode of excitation of the helium atom.

2.2   Classical Mechanical Theory of the Hanle Effect

In order to discuss the Hanle effect classically one uses, as a
model for the atom, an oscillating electric dipole which possesses a
magnetic dipole moment, μ , perpendicular to the dipole axis.

If this dipole is set into oscillation along the x-axis with a
frequency ν it will emit radiation in a direction perpendicular to
the dipole axis. The electric vector of the emitted radiation will be
parallel to the dipole axis (see Fig. 2).   If one observes this
radiation along the z-axis, the signal will appear polarized 100% in the
x direction.

Now, one places a magnetic field $\underline{H} = H \hat{K}$ along the z-axis. If we
assume μ to be of the form $\underline{\mu} = \gamma \underline{L}$, where $\underline{L}$ is the angular momentum,
the magnetic field puts a torque on the dipole, and causes it to precess
about the z-axis with an angular frequency $\omega = \mu H$. Now, the angle to
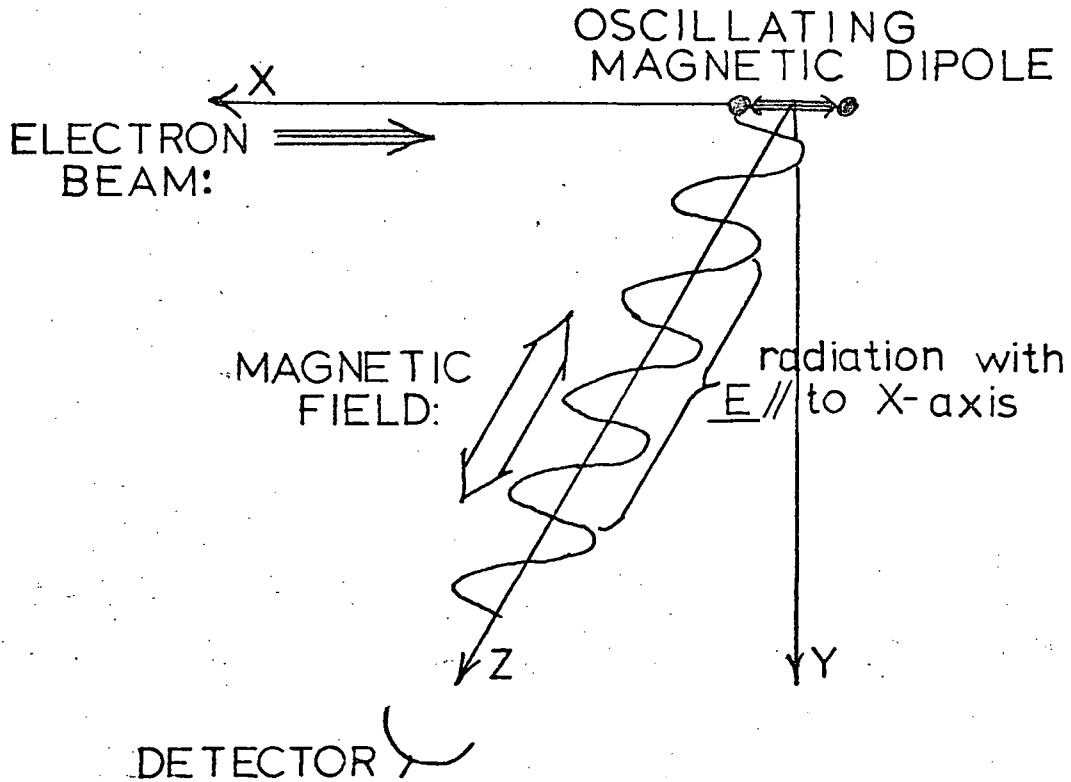
FIG. 2--Classical Radiating Dipole

the z-axis of the $\underline{E}$ vector of the emitted radiation will be:

$$\ominus(t) \;=\; \omega\, t \;=\; \mu\, Ht \tag{1}$$

The amplitude of the emitted radiation is radiation damped, with a time constant $2\,\tau$, where τ represents the mean life of the upper state involved. Thus the observer, looking along the z-axis, will see time dependent electric field components of the form:

$$A_x(t) \;=\; A_o \cos(\omega\, t)e^{-i(\nu t + \delta)}\, e^{-t/2}$$

$$A_y(t) \;=\; A_o \sin(\omega\, t)e^{-i(\nu t + \delta)}\, e^{-t/2} \tag{2}$$

or the intensity of radiation with electric vectors along the x- and y-axis is:

$$I_x(t) = A_0 \cos^2(\omega t) e^{-t/\tau}$$

$$I_Y(t) = A_0 \sin^2(\omega t) e^{-t/\tau} \tag{3}$$

Usually one observes, over a long period of time, T, in comparison to τ. Now the intensities become:

$$I_x = \int_0^T I_x(t)dt = \int_0^\infty I(t)dt$$

$$I_Y = \int_0^T I_Y(t)dt = \int_0^\infty I(t)dt \tag{4}$$

The polarization "P" is defined to be:

$$P = \frac{I_x - I_Y}{I_x + I_Y} \tag{5}$$

Substituting Equation 4 into Equation 5:

$$P = \frac{\int_0^\infty (\cos^2 \omega t - \sin^2 \omega t) e^{-t/\tau} dt}{\int_0^\infty e^{-t/\tau} dt}$$

performing the integration and substituting $\omega = \mu H$ in Equation 6 we find

$$P = \frac{1}{1 + (2\mu H \tau)^2} \tag{7}$$

If one plots "P" as a function of H, a curve of the form shown in Fig. 3 is obtained.

The lifetime, τ, can be found by noticing that when $\frac{P(H_{\frac{1}{2}})}{P(0)} = \frac{1}{2}$ is given by:

$$\tau = \frac{1}{2\mu H_{\frac{1}{2}}} \tag{8}$$

POLARIZATION

MAGNETIC FIELD
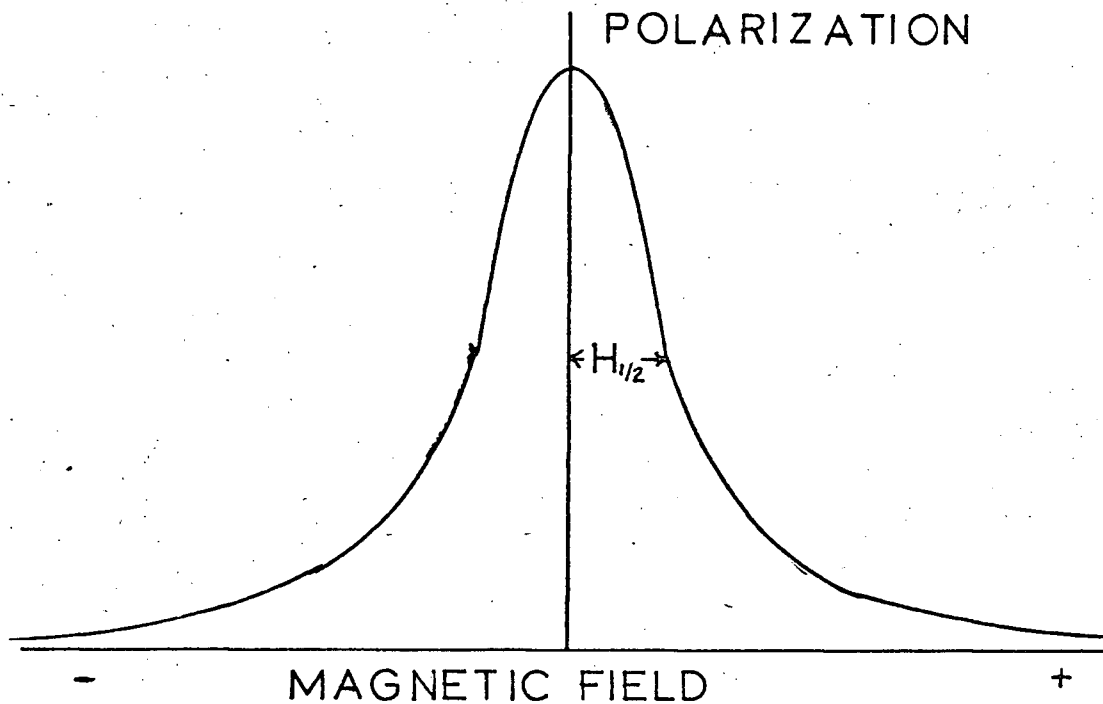
FIG. 3--Typical Polarization
Curve

In the case of an atom, one must evaluate the magnitude of the

magnetic moment $\mu = g\mu_0$, where μ_0 is the Bohr magniton:

$$\mu_0 = \frac{e}{2mc}$$

In the preceding description it is implied that the only depolar-

ization can also be caused by a collision of one atom with its neighbour.

Another constraint on this theory is the time of the excitation

process. That is, it must be short in comparison to τ . Our excitation

process by electron collision is of the order of 10^{-14} seconds.

2.3   Quantum-Mechanical Description of the Hanle Effect

In 1924 Hanle observed the depolarization of polarized light by a

magnetic field.[3]   In 1933 Breit derived a quantum mechanical expression

which described the Hanle effect.[4]   Then in 1959 Franken[5] rederived

it for level crossing experiments (zero field level crossing is called the Hanle effect).

Breit was puzzled with the lack of completeness in the mathematical description for the following situation:

One considers a four-level system, with ground states $|a\rangle$ and excited states $|b\rangle$, $|c\rangle$, and $|d\rangle$. (See Fig. 4.) Let states $|b\rangle$ and $|c\rangle$ be Zeeman sublevels of one state, then the separation between these states will be a function of the magnetic field. Now there are three cases which have to be explained;

   i)   completely separate states $|b\rangle$ and $|c\rangle$

   ii)   completely overlapping states $|b\rangle$ and $|c\rangle$

   iii)   an intermediate situation between case (i) and (ii).
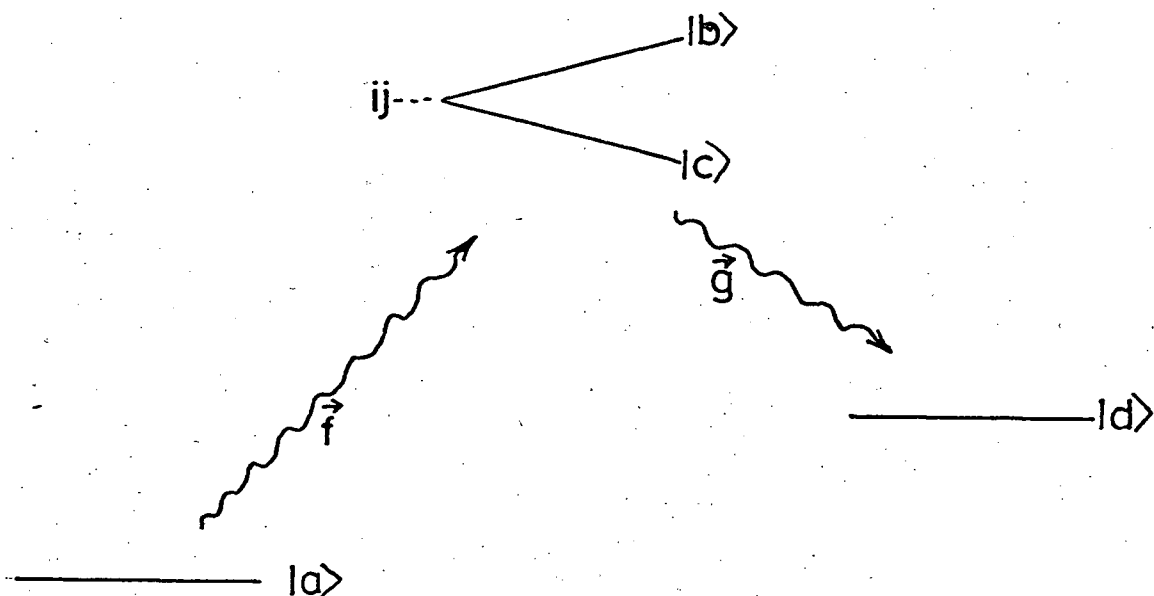
FIG. 4--Four Level System

Before 1933, cases (i) and (ii) were completely explained mathematically. But, there was no expression for case (iii). Breit explained the third case. Below, I will give the expression for all three cases.[6]

F(fg) is the radiation emitted when light of polarization $\underline{f}$ excites state $|a\rangle$ to states $|b\rangle$ and $|c\rangle$ and then decays down to state $|d\rangle$ by emitting light of polarization $\underline{g}$.

$$\text{case (i)} \quad R(fg) = |f_{ab}\, g_{bd}|^2 + |f_{ac}\, g_{cd}|^2 \qquad (9)$$

$$\text{case (ii)} \quad R(fg) = |f_{ab}\, g_{bd} + f_{ac}\, g_{cd}|^2 \qquad (10)$$

$$\text{case (iii)} \quad R(fg) = c \sum_{ij} \frac{f_{ia}\, f_{aj}\, g_{id}\, g_{dj}}{1 - i\tau(E_i - E_j)\hbar} \qquad (11)$$

The expression for case (iii) is called the Breit formula, where j and i refer to the Zeeman sublevels of the excited state. E_i is the energy of the ith excited substate. f_{ia} and g_{id} are dipole transition-matrix elements between the states in question, given by:

$$f_{ia} = \langle \alpha, J, i | \underline{f} \cdot \underline{r} | \alpha', J-1, a \rangle$$
$$g_{id} = \langle \alpha, J, i | \underline{g} \cdot \underline{r} | \alpha', J-1, d \rangle$$

where $\underline{r}$ is defined to be a vector along the dipole axis. The above expressions for f_{ia} and g_{ia} are for dipole transitions which stipulate that $\Delta J = \pm 1$. In this experiment electron excitation was used to excite the helium atom from a ^1S state (J = 0) to a ^1D state (J = 2). Thus the expression for f_{ia} cannot be used and for the time being, will be replaced with Q_{ia} which will be dealt with later.

For a large magnetic field, $E_b - E_c \gg 1$, the expression for R(fg) reduces to the same expression given for case (i) earlier. For a zero magnetic field $E_b - E_c = 0$ and R(fg) reduces to case (ii) as is expected. Now, from the expression for R(fg) we can see that for a moderate magnetic field, the factor $[1 - i\tau(E_i - E_j)/\hbar]^{-1}$ remains in some of the terms.

Hence $R(fg)$ is dependent on both τ and the magnetic field. Therefore, by controlling the magnetic field one is capable of solving for τ .

In order to adapt the Breit formula for this experiment, it is broken up into two parts; one dependent and the other independent of the magnetic field. The independent part is segregated by noticing that in terms when $i = j$; $E_i - E_j = 0$, the respective terms are independent of the magnetic field. These terms are represented by R_o;

$$R_o = \sum_i Q_{ia}{}^2 \; g_{id}{}^2 \tag{12}$$

Rewriting Equation (11) in the two parts as stated above and setting:

$$Q_{ia} \, Q_{aj} \, g_{id} \, g_{di} = A(aijd) \tag{13}$$

$$R(fg) = R_o + \sum_{i \neq j} \frac{A(aijd)}{1 - i\tau(E_i - E_j)\hbar} \tag{14}$$

$$R(fg) = R_o + \sum_{i > j} \frac{A}{1 - i\tau(E_i - E_j)\hbar} + \frac{A*}{1 + i\tau(E_i - E_j)\hbar}$$

$$R(fg) = R_o + \sum_{i > j} \frac{1}{1 + \tau^2(E_i - E_j)^2} \left[(A + A*) + \frac{i\tau(E_i - E_j)}{\hbar} (A - A*) \right] \tag{15}$$

It can be shown that $A = 0$ unless $|m_i - m_j| = 2$, and that A has the form $A = A_o \exp(2i\phi)$ where ϕ is the angle between the x and y axes of the atom's coordinate system and the ξ and ζ axes of the observer's coordinate system. Assuming that the levels exhibit a linear Zeeman effect in a magnetic field, then:

$$E_i = E_J + \frac{\hbar geH \mu_o m_i}{2mc}$$

hence; $$E_i - E_j = \frac{\hbar geH \mu_o}{mc} \tag{16}$$

Substituting Equation (16) into Equation (15) and simplifying,

$$R(fg\phi) = R_o + \sum_{i > j} \frac{2 A_o}{1 + (\frac{geH\tau}{mc})^2} \left[\cos 2\phi - \frac{geH\tau}{mc} \sin 2\phi \right] \quad (17)$$

The polarization, with respect to the   axis is defined to be:

$$P = \frac{R(\phi) - R(\phi + \pi/2)}{R(\phi) + R(\phi + \pi/2)} \quad (18)$$

Substituting Equation (17) into Equation (18) and simplifying, one gets:

$$P = \frac{1}{1 + (\frac{geH\tau}{mc})^2} \cdot \frac{2}{R_o} \sum_{i > j} A_o \left(\cos 2\phi - \frac{geH\tau}{mc} \sin 2\phi \right) \quad (19)$$

$$P = \frac{P_o}{1 + (\frac{geH\tau}{mc})^2} \cdot \left(\cos 2\phi - \frac{geH\tau}{mc} \sin 2\phi \right) \quad (20)$$

where $P_o = \frac{2}{R_o} \sum_{i > j} A_o (aijd)$

Comparing Equation (12) with the expression for the polarization derived classically (Section 2.2), one can see by setting $\phi = 0$, (this was done automatically in the classical explanation in order to simplify it) the two expressions are the same, except for a difference in the definition of P_o.

2.4   The Excitation Matrix Elements

In order to apply Equation (12), we must find an expression for the perturbation matrix elements Q_{ia}. Even though laws governing electron atom collisions at non-relativistic energies are completely known, the calculation of low energy scattering cross-sections is extremely complex and has only been attempted for the most simple atomic cases. Referring to Equation (12), it should be noted that as long as $P_o \neq 0$ and is independent of the magnetic field it will have no effect

on the shape of the curve. Since it was experimentally observed that $P_o \neq 0$ there was no need to calculate Q_{ia}.

2.5   The Helium Atom

A diagram of the pertinent levels of the helium atom is given in Fig. 5. The ^3S state normally has a relatively large lifetime because dipole transition from a triplet to a singlet state in helium is forbidden. Thus after a period of time this state becomes populated. This could make the mode of excitation as is shown by the dotted lines in Fig. 5. But there are the following complications which make the previous mode unlikely. Firstly, since the atom in the triplet state frequently collides with the walls of the discharge cell, its lifetime is shortened. And secondly, since the electron density is small, there is a relatively long period of time between collisions of atoms and electrons. Thus the population of the ^3S state is considerably smaller than expected. From the above argument, the transition ^1S - ^1D (full line in Fig. 5) would be more probable. A suitable explanation would say that a percentage of the atoms are excited to the ^1D states directly from the ^1S ground state, and a percentage is excited via the metastable ^3S state. The proportion depends on the density of electrons with energies of 20 ev. in the discharge cell.
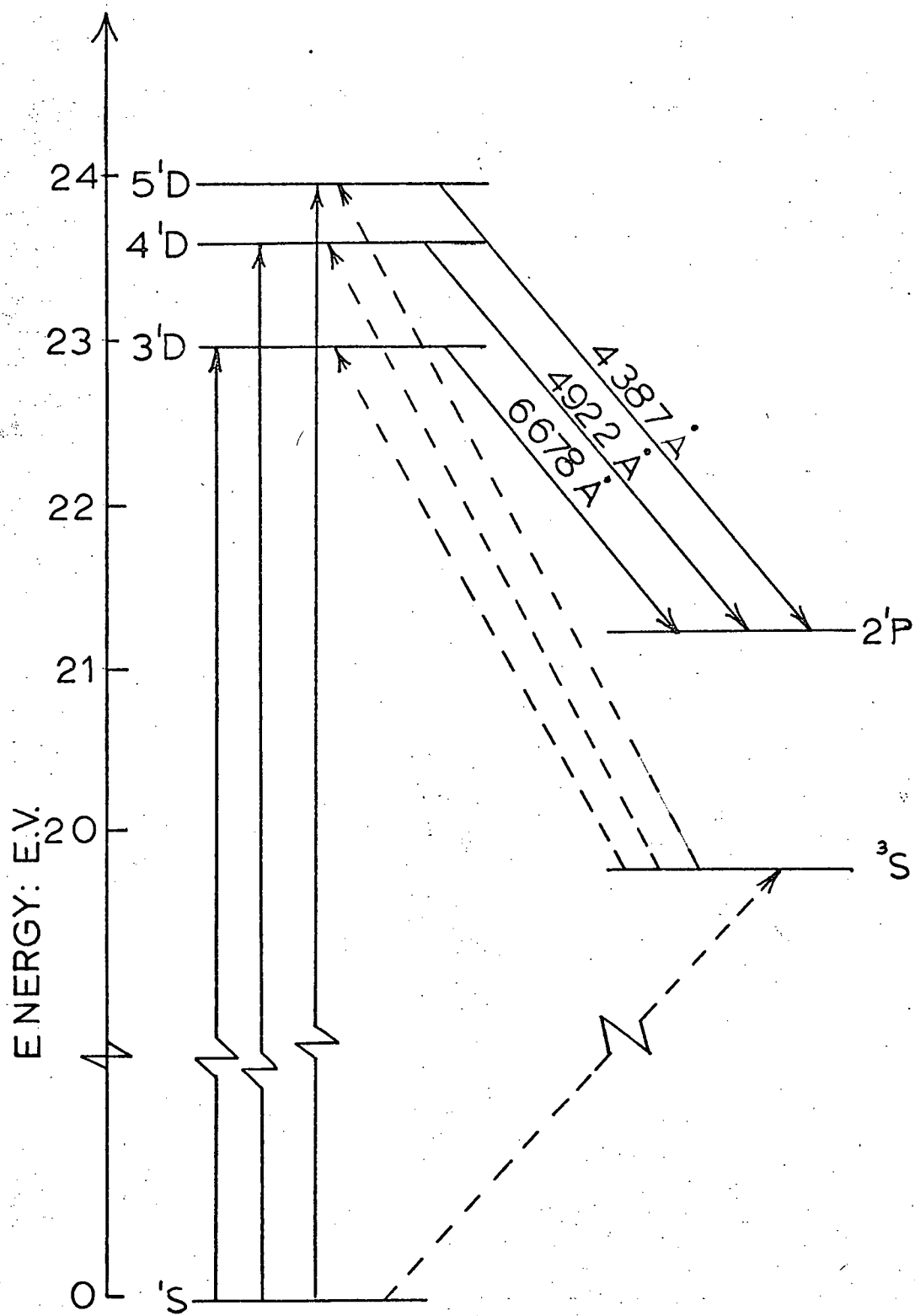
FIG. 5--Energy Levels of Helium Atom

CHAPTER III

EXPERIMENTAL DETAILS

3.1 Experimental Arrangement[7]

The experimental system required to detect the Hanle effect described earlier, is composed of four main parts; 1) a cell containing a radio frequency excited discharge, 2) a homogeneous variable magnetic field in the discharge region, 3) an optical filter which passes only the spectral line of interest, and 4) a device for detecting and measuring polarization. A schematic diagram of the apparatus is shown in Fig. 6.

The discharge cell is placed between a pair of capacitor plates which lie parallel to the y-z plane. These plates are connected to a power supply which produces a radio-frequency electric field of the form $\underline{E} = (E_o \cos \omega t)\hat{i}$, thus causing free electrons to oscillate in the $\pm x$ direction.

A homogeneous magnetic field is produced by two sets of Helmholtz coils. One is used to cancel the earth's magnetic field in the y direction, and the other is used to produce a variable magnetic field $\underline{H} = H\hat{k}$ in the z direction. The light travelling in the z direction is passed through a monochromator which is set to transmit the wavelength of interest. This radiation is detected by using a photomultiplier, the output of which is fed into the signal channel of a lock-in amplifier.

To detect the polarization of the signal, a rotating quarter-wave plate was used. Before entering the monochromator, the signal passes through a rotating quarter-wave plate, and a fixed polaroid with its

MONOCHROMATOR

CAPACITOR PLATES

POLAROID

P.M.

REFERENCE

ROTATING
λ/4 PLATE

HELMHOLTZ
COILS

X-AXIS

Z-AXIS

LOCK-IN AMP.

X-Y RECORDER

FIELD-
SWEEP
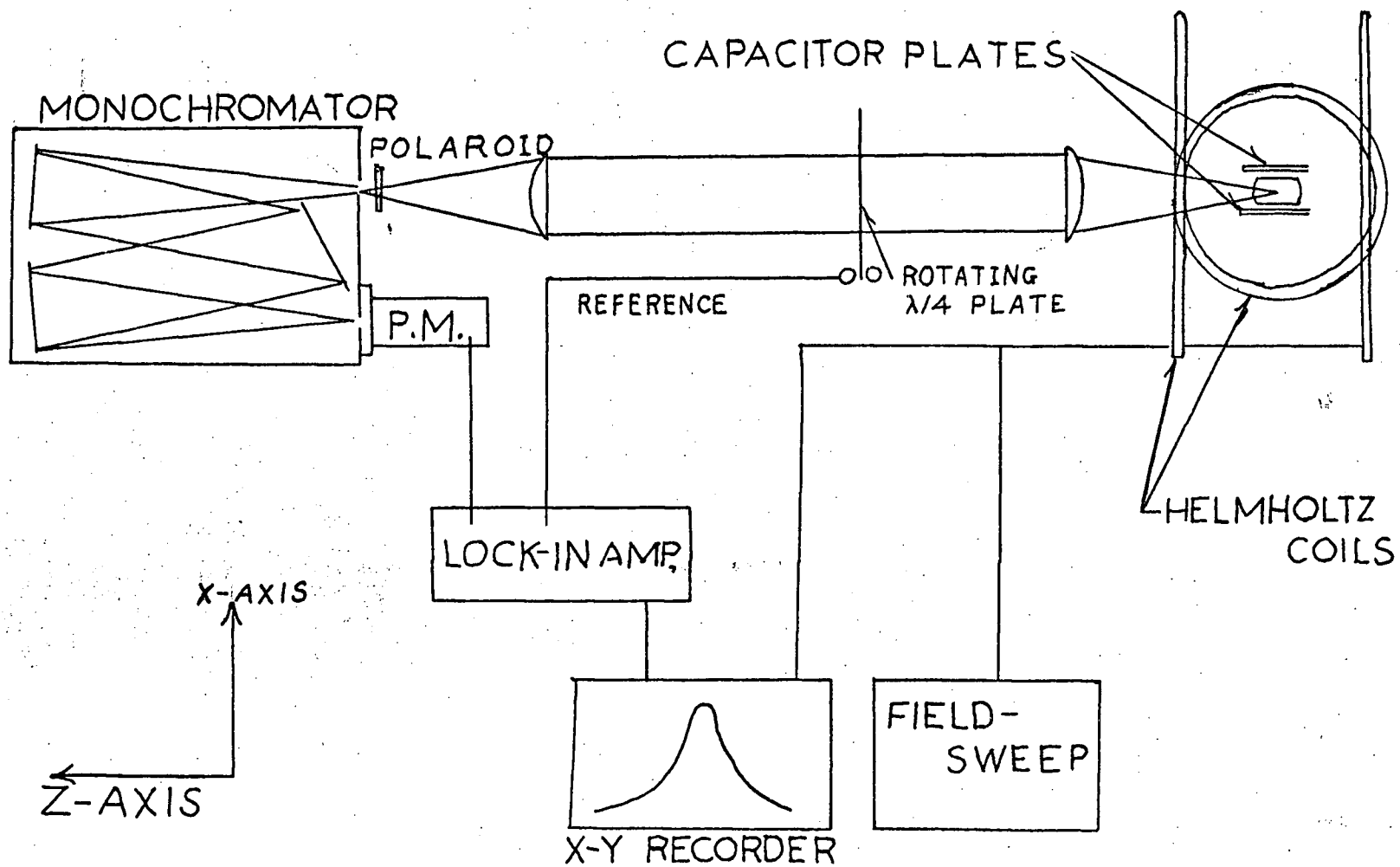
FIG. 6--Apparatus

axis in the y direction. The polarized component of the light is thus modulated at four times the rotational frequency of the quarter-wave plate. This rotational frequency provides a reference signal for the lock-in amplifier (see Section 3.5). The output of the phase-sensitive detector now shows the degree of polarization. The output of the lock-in amplifier is connected to the y-channel of the x-y recorder. The x channel is controlled by the voltage across the Helmholtz coils producing a field $\underline{H} = H\hat{k}$. These coils are driven by a power supply and an amplifier whose output is slowly swept to produce fields of the form $H = H_o + \beta t$ where $H_o \simeq - 15$ gauss and $H_{max} \simeq + 15$ gauss.

3.2   The Discharge

The discharge apparatus consisted of a cylindrical pyrex discharge cell 5 cm in diameter and 2.5 - 3 cm in length. The cell was connected to the vacuum system by a 1 cm O.D. pyrex tube as shown in Fig. 9. The ends of the discharge cell are slightly convex in shape to provide mechanical strength against air pressure. A circular brass plate of 7 cm in diameter is placed at either end so that it extends about 1 cm beyond the edges of the cell. The plates were parallel to the z-y plane. The output of a radio frequency transmitter is coupled to these plates in a manner described in Section 3.7.

The cell and plates are shown full scale in Fig. 7. For convenience, the coordinate axes used throughout the discussion are also shown.

The discharge is assumed to consist of a dilute gas of neutral atoms and a much smaller number of free electrons and ions. The motion of the electrons in a radio-frequency electric field, assuming a complete
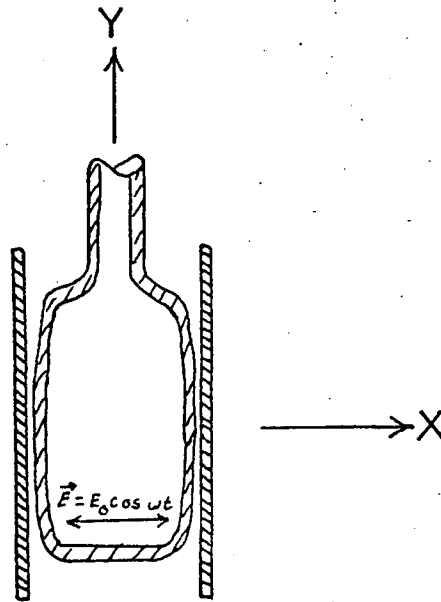
FIG. 7--Cross-section of Discharge Cell and Capacitor Plates

absence of collisions and a zero magnetic field, is governed by:

$$m\ddot{x} = eE_o \cos \omega t$$

$$x = \frac{eE_o}{m\omega^2} \cos \omega t$$

and the kinetic energy K.E. is given by

$$K.E. = \frac{1}{2} m\dot{x}^2 = \frac{1}{2m} (\frac{eE_o}{\omega})^2 \sin^2 \omega t$$

The application of a small magnetic field $\underline{H} = Hk$ yields:

$$m\ddot{x} = eE_o \cos \omega t - eH\dot{y}$$

$$m\ddot{y} = eH\dot{x}$$

Solving these equations:

$$x(\omega t) = -\frac{eE_o}{m} (\frac{1}{\omega^2 - \nu^2}) \cos(\omega t)$$

$$y(\omega t) = \frac{\nu}{\omega} x(\omega t + \pi/2)$$

where $\nu = \dfrac{eH}{m}$

This describes an electron moving in an ellipse whose ratio of major to minor diameter is $\dfrac{\omega}{\nu}$. For our case — (see Table I).

In order for the above description to meet the conditions of the discharge cell, three conditions must be satisfied; 1) The mean free path of the electron should exceed the amplitude of its motion.

2) Collisions of electrons with the walls of the discharge cell must also be rare events. This merely means that any dimension of the discharge cell ought to exceed considerably, the amplitude of the electron's motion.

3) Electrons must be sufficiently energetic to sustain the discharge; that is, they must have sufficient energy to ionize the occasional molecule in order to make up for electrons lost by recombination.

Table I lists some of the properties of the motion of the electrons in an oscillating electric field.

TABLE I.--PROPERTIES OF ELECTRON MOTION IN AN R.F. ELECTRIC
D.C. MAGNETIC FIELD

Frequency $(*10^6$ Hz)	E Required To Produce K.E.$_{max}$ -20ev.	Amplitude of Electron Motion (Major Diameter)	Minor Axis to Major Axis Ratio in 10 Gauss Magnetic Field
200	200 V/cm	2 mm	.035
500	500 V/cm	0.8 mm	.014

In order to see how well the first condition is satisfied we compute the mean free path, L, between molecule of cross-section , dis-

tributed with a density ρ ; $L = \frac{1}{\rho \sigma}$. Then at a density of 6.68 $10^{14}/cm^3$ and assuming a cross-section of 10Å; $L \simeq 1$ cm. From these figures we see that the condition is fairly well satisfied.

By consulting Table I, one can see that condition (2) is easily satisfied for the discharge cell that was used.

Condition 3 is satisfied when the pressure in the cell is greater than .060 mmHg. (This value was found experimentally.)

3.3 The Optical System

The light from the discharge passes through a pair of plano-convex lenses, one of which is placed at its focal length away from the discharge, the other is placed at its focal length away from the entrance slit of the monochromator. A rotating quarter-wave plate is placed in the parallel beam of light between the two lenses (see Fig. 6). The aperture of the quarter-wave plate is large enough not to constitute a "stop" in the optical system (see Fig. 9). In front of the slit of the monochromator a piece of polaroid was placed perpendicular to the axis of observation. Observations were performed at wave lengths of 4387Å, 4922Å, and 6678Å. The monochromator, an F/8 Spex, one metre instrument had, when used in second order, a dispersion of $\simeq 6$Å/mm, and a resolution of better than 0.1Å. Since there were no spectral lines within 30Å of the above mentioned lines, it was possible to use slitwidths of 0.3 mm yielding a resolution of $\simeq 2$Å. The rotating quarter-wave plate followed by a polaroid with its axis of acceptance in the y direction, was used to detect the polarization of the light, instead of what seems more straightforward, a rotating polaroid. The former method was used because the efficiency of the monochromator was found to depend upon the polar-

ization of the emitted light. By placing the polaroid in front of the

entrance slit of the monochromator, the effect of the monochromator was

cancelled. A detailed calculation in Appendix (1) will show that when

a signal is emitted from the discharge, which is polarized at an angle

Θ to the x-axis, the system explained above produces a signal of the

form:

$$V(t) = \frac{A_o^2}{2} \left\{ -1 + \left[\frac{\cos 4\omega t + 1}{2} \right] \cos 2\Theta - \frac{1}{2} \sin 4\omega t \sin 2\Theta \right\}$$

where ω is the frequency of the rotating quarter-wave plate.

3.4   Lock-In Amplifier

The lock-in amplifier consists of a tuned pre-amplifier with a Q

of about 10 and a phase sensitive detector. The lock-in amplifier used

in this experiment is a Princeton Applied research Model 120, which has

a linearity of 1% and a gain of 10^4. The output is D.C. ± 10V at full

scale. In the mode it was used, the reference signal triggers an

internal sinusoidal reference signal. In this experiment a three-second

time constant was used throughout.

With the chopped input signal from the photomultiplier,

the output signal of the lock-in amplifier is proportional to the

polarization, P, of the emitted light referred to the x-axis. With an

input signal V(t) an output signal, S, is of the form:

$$S \propto \frac{2\pi\omega}{T} \sum_{n=1}^{T/2\pi\omega} \int_{2n}^{2(n+1)\pi} V(t)\cos(\nu t - \phi)\,d(\nu t)$$

where: ϕ is the selected phase angle

ν is the tuned frequency

T is the time constant

So long as T is sufficiently large, incoherent signals will average to zero. Substituting in the expression for V(t), determined earlier as the signal from the photomultipler (see Section 3.3):

$$S \propto \int_0^{2\pi} \left\{ \left[\frac{1 + \cos 4\omega t}{2} \right] \cos 2\Theta + \frac{1}{2} \sin 4\omega t \sin 2\Theta - 1 \right\} \cos(\nu t - \phi) d(\nu t)$$

where ω is the frequency of rotation of the quarter-wave plate. From the explanation in Section 3.5 it can be seen that $\nu = 4\omega$, (i.e. four cycles are gone through for each revolution of the quarter-wave plate). By setting $\phi = 0$

$$S \propto \int_0^{2\pi} \left\{ -\cos 4\omega t + \frac{\cos^2 4\omega t \cos 2\Theta}{2} + \frac{\cos 4\omega t \cos 2\Theta}{2} \right.$$
$$\left. + \frac{\sin 4\omega t \cos 4\omega t \sin 2\Theta}{2} \right\} d(4\omega t)$$

$$S \propto \cos 2\Theta = \cos^2 \Theta - \sin^2 \Theta = P$$

Thus the output signal, S, of the phase sensitive detector is proportion to the polarization, P, of the emitted light.

3.5   Rotating Quarter-Wave Plate and Reference Signal

The rotator is shown in Fig. 8. A quarter-wave plate is glued to a two-inch I.D. brass pipe which is fitted tightly inside large ball-bearings. A sewing machine belt is laid over the pipe and the motor pulley rotates the quarter-wave plate. The motor, model CH3GRH, Universal Electric Company, runs at 1050 r.p.m. and delivers .05 H.P. The motor pulley has a 1.2 inch diameter. Thus the quarter-wave plate is rotated at approximately 10 cycles per second.

The revolving quarter-wave plate also furnishes the reference

QUARTER-WAVE PLATE

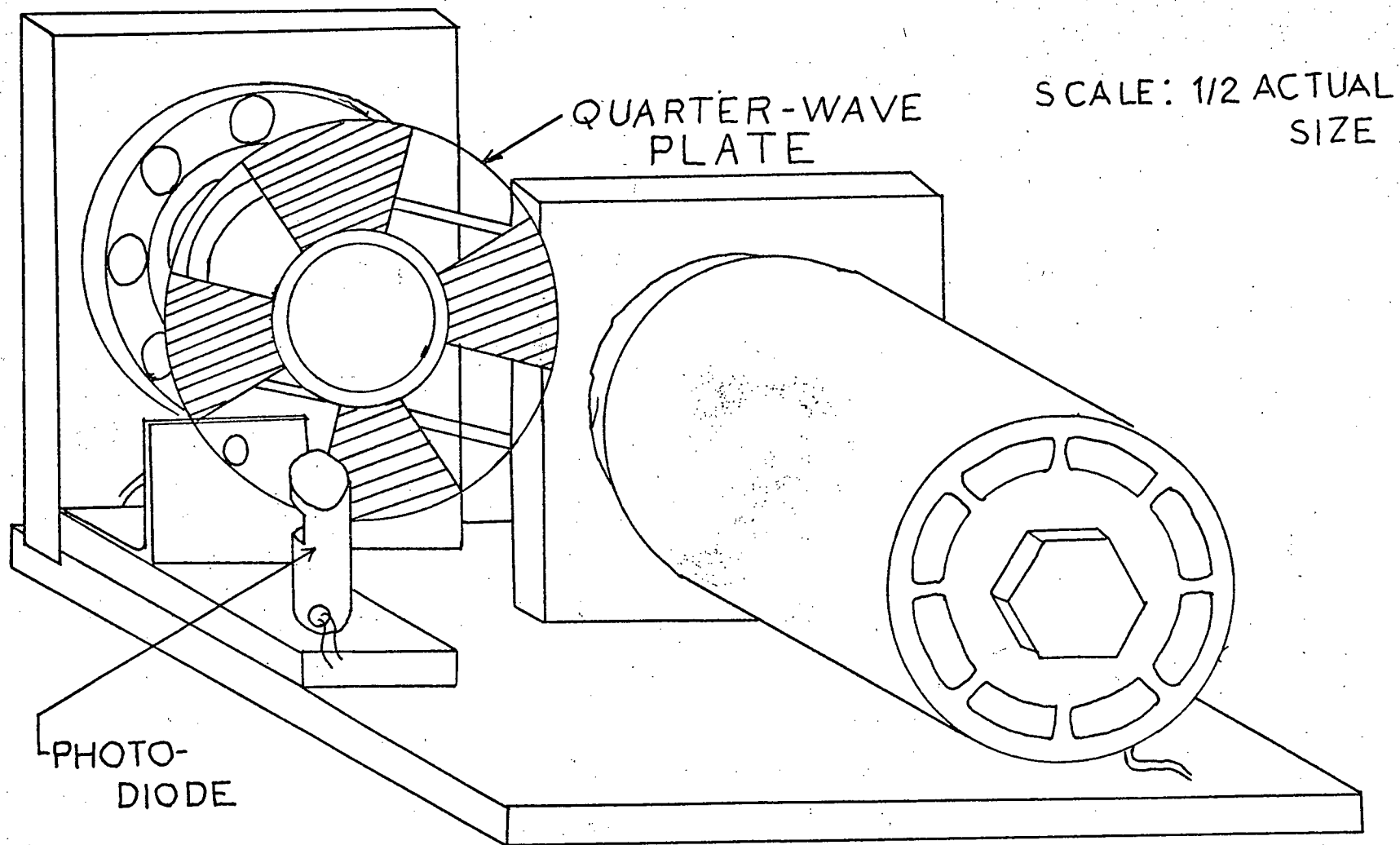SCALE: 1/2 ACTUAL SIZE

PHOTO-DIODE

FIG. 8--Quarter-Wave Plate Rotator

signal; painted sections were symmetrically placed around the perimeter of the quarter-wave plate in order to interrupt a light signal falling on a photodiode at a frequency 4ω (see Fig. 8).

3.6   Vacuum System

The vacuum system is shown in Fig. 9. It is a conventional glass system pumped by a "Cenco-Hyvac 14" mechanical pump which is capable of reducing the pressure in the system to less than 5×10^{-4} mm Hg when a liquid nitrogen cold trap was used to prevent backstreaming of pump oil. Helium gas was leaked into the system through a needle valve. The leakage rate established the equilibrium pressure of the system.

Starting from the reduction valve on the pressure bottle, helium at $\simeq 2$ pounds per square inch above atmospheric pressure was passed through a flexible rubber hose to a cold trap filled half-way with activated charcoal. This cold trap was utilized to purify the commercial helium that was used. From there, the gas proceeds through some more flexible rubber hose to the needle valve and from there, at low pressure, to the discharge cell. About halfway between the discharge cell and the needle valve, a Pirani gauge was attached. Just above the discharge cell a McLeod gauge was attached. Both of these were connected to the system via glass stopcocks. Proceeding downstream from the discharge cell another cold trap was encountered before the gas was pumped out by the mechanical pump. All connecting glass tubing has an inside diameter of 7 mm. Some flexibility in the position of the discharge cell was provided by the ground glass swivel joints, by which it was connected to the vacuum system.

When data was being taken, the pressure was measured with the

NEEDLE VALVE

MCLEOD GAUGE

TO CHARCOAL TRAP

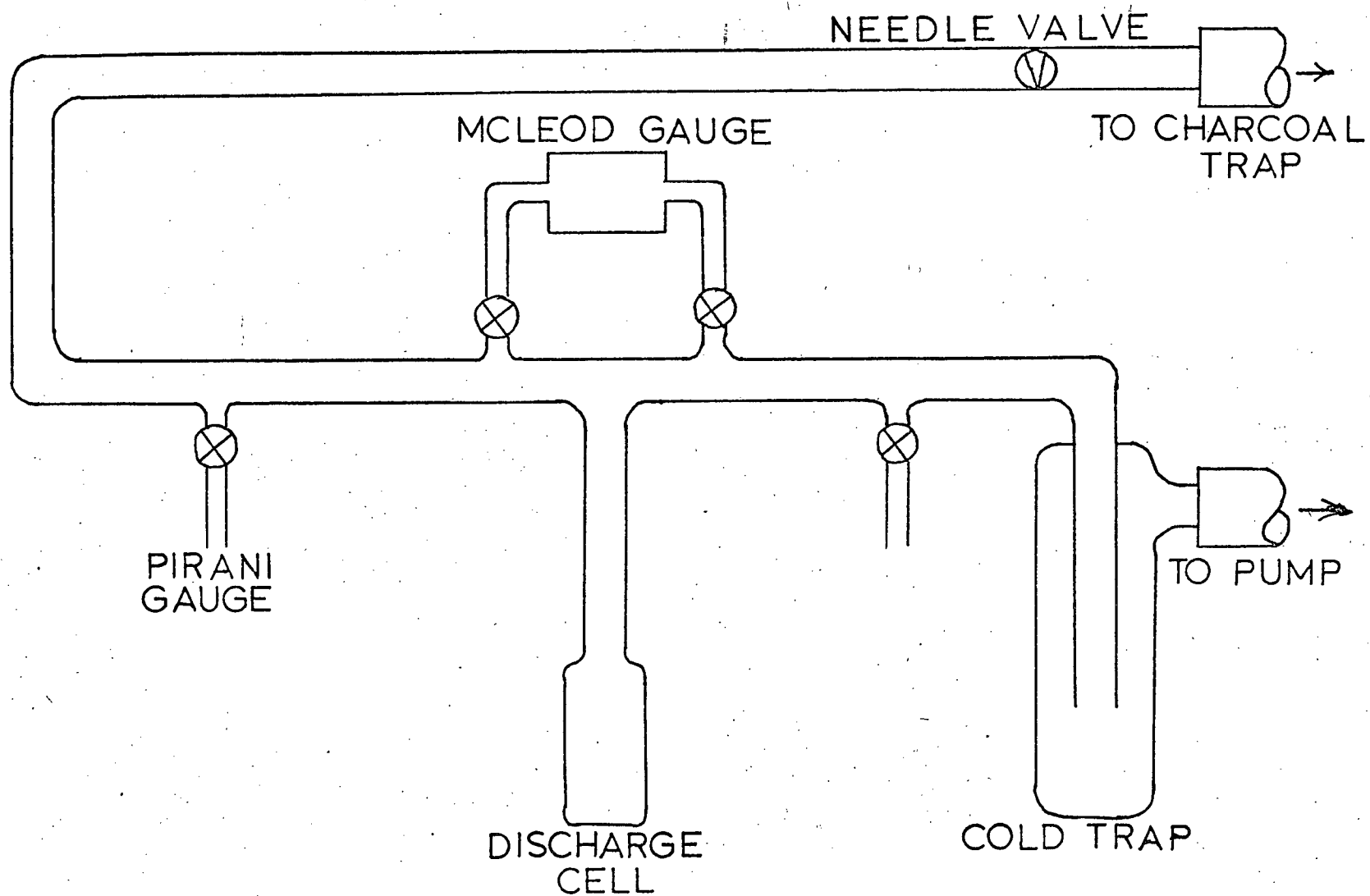PIRANI GAUGE

TO PUMP

DISCHARGE CELL

COLD TRAP

FIG. 9--Vacuum System

McLeod gauge before and after each run. It was noticed that, for

pressures less than .075 mm Hg, when the stopcock to the McLeod gauge

was opened the intensity of the discharge changed in appearance to the

naked eye. Thus the stopcock was opened only while pressure readings

were taken, then it was closed and we waited about five minutes until

the discharge returned to a steady state before the run was taken. The

Pirani gauge was used as a check for pressure fluctuations. Runs were

taken for various pressures between .300 and .050 mm Hg. The pressure

readings were accurate to $\pm 7\%$.

The discharge was periodically observed with a small hand spectro-

graph in order to check the purity of the spectrum.

3.7   R.F. Supplies and Coupling

The source was a 450 Mz transmitter. It consisted of an R.C.A.

M.I. -17436-1 transmitter used as a "driver" and a Canadian Marconi,

Model 163-107 high frequency power amplifier. With an output impedance

of 50Ω an output power of approximately 50w was transmitted. The R.F.

voltage available is 50 V. Since we needed a field of order, 400 V/cm.

between the discharge capacitor plates, and the plates were spaced at

3 cm, then 1200 V is required. Voltages of this order were obtained by

the "Γ matched" resonant circuit shown in Fig. 10. A length of RG 8-U

cable carried the power to this circuit. By adjustment of the contact

point A, (see Fig. 10), an approximate impedance match between the

resonant circuit and the transmission line may be obtained. The circuit

is tuned to resonance by moving the cross-bars closer together or further

apart, while keeping them equidistant from the capacitor plates. The

advantage of using such a high frequency source is that it has a negligible

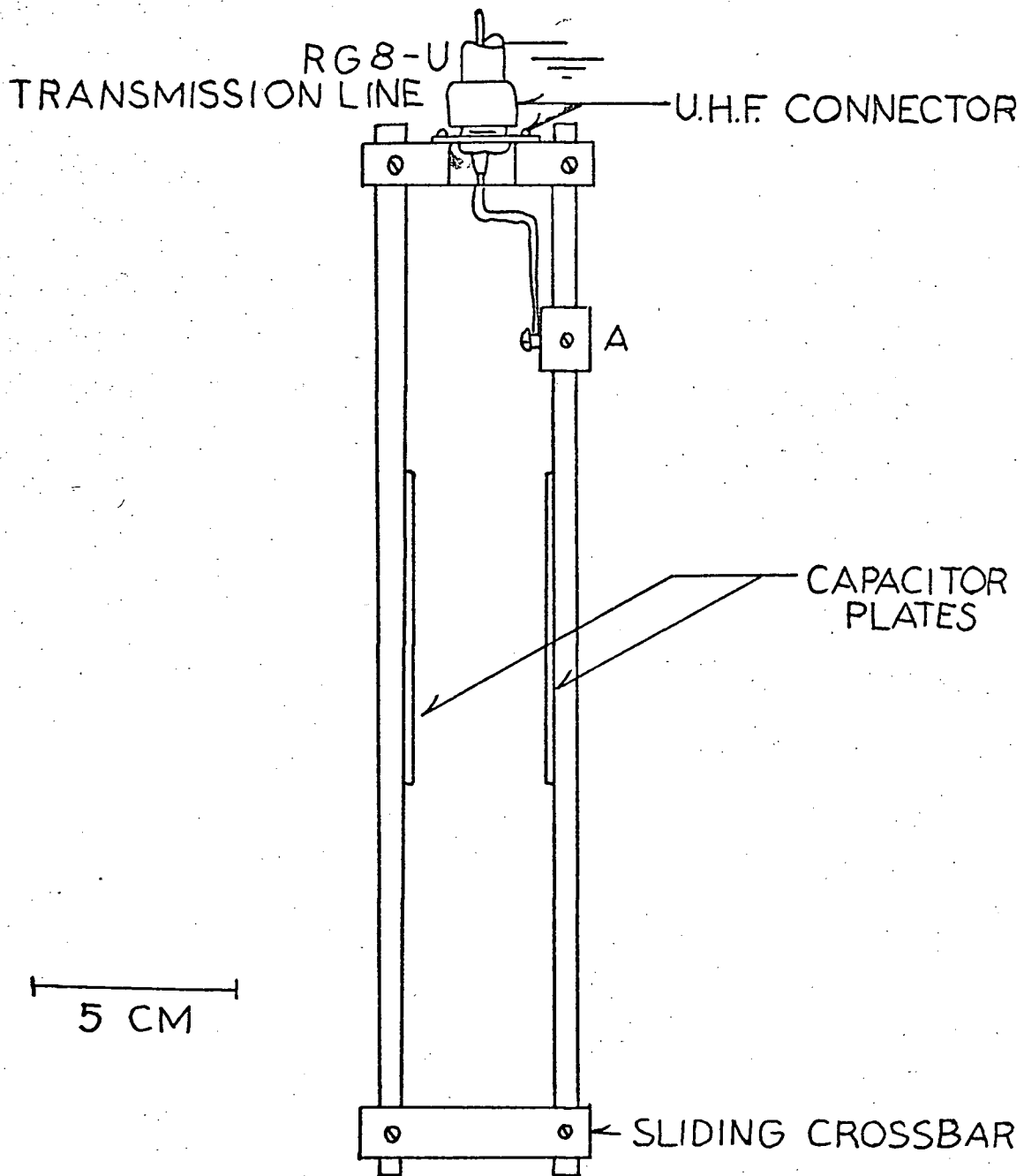effect on other parts of the apparatus such as the phase sensitive

FIG. 10-- - Matched Resonant Circuit

detector or the x-y recorder.

3.8   Helmholtz Coils

The applied magnetic field in the x-direction was designed to be homogeneous in the area of the discharge cell to about 1 part per 4,000. In general, inhomogeneity near the centre of the Helmholtz coils are of the order $(\frac{r}{R})^4$; where "r" is the radius of the test area (discharge cell), and "R" is the radius of the coils. Therefore, Helmholtz coils with a diameter of 37 cm and a spacing of 18.5 cm were used in series. These coils each had 100 turns of #18 wire.

The current delivered to these Helmholtz coils is supplied by a pair of "EICO 1064" power supplies and regulated by a D.C. power amplifier, whose schematic is shown in Fig. 11. The amplifier delivers up to 7A of either polarity into a 1 Ω load with reasonable linearity; has a voltage gain of approximately unity and an input impedance of approximately 10K Ω. This enables the coils to give a magnetic field of anywhere between $\pm$15 gauss.

The sweep of the magnetic field is controlled by an R.C. circuit whose output is fed into a preamplifier before going into the circuit, as shown in Fig. 12. The time constant of the R.C. circuit is 20 minutes, thus by varying the gain of its preamplifier, the sweep time can be selected between 3 and 20 minutes. Most runs were done with a sweep time of 7 minutes.

The calibration of these coils was done with a "Bell 240" Hall gaussmeter. The accuracy of this gaussmeter was tested by using it to measure a magnetic field of $\cong$ 1.5K gauss that was known to be accurate to 0.5%. The "Bell 240" Hall gaussmeter measured the strength of this
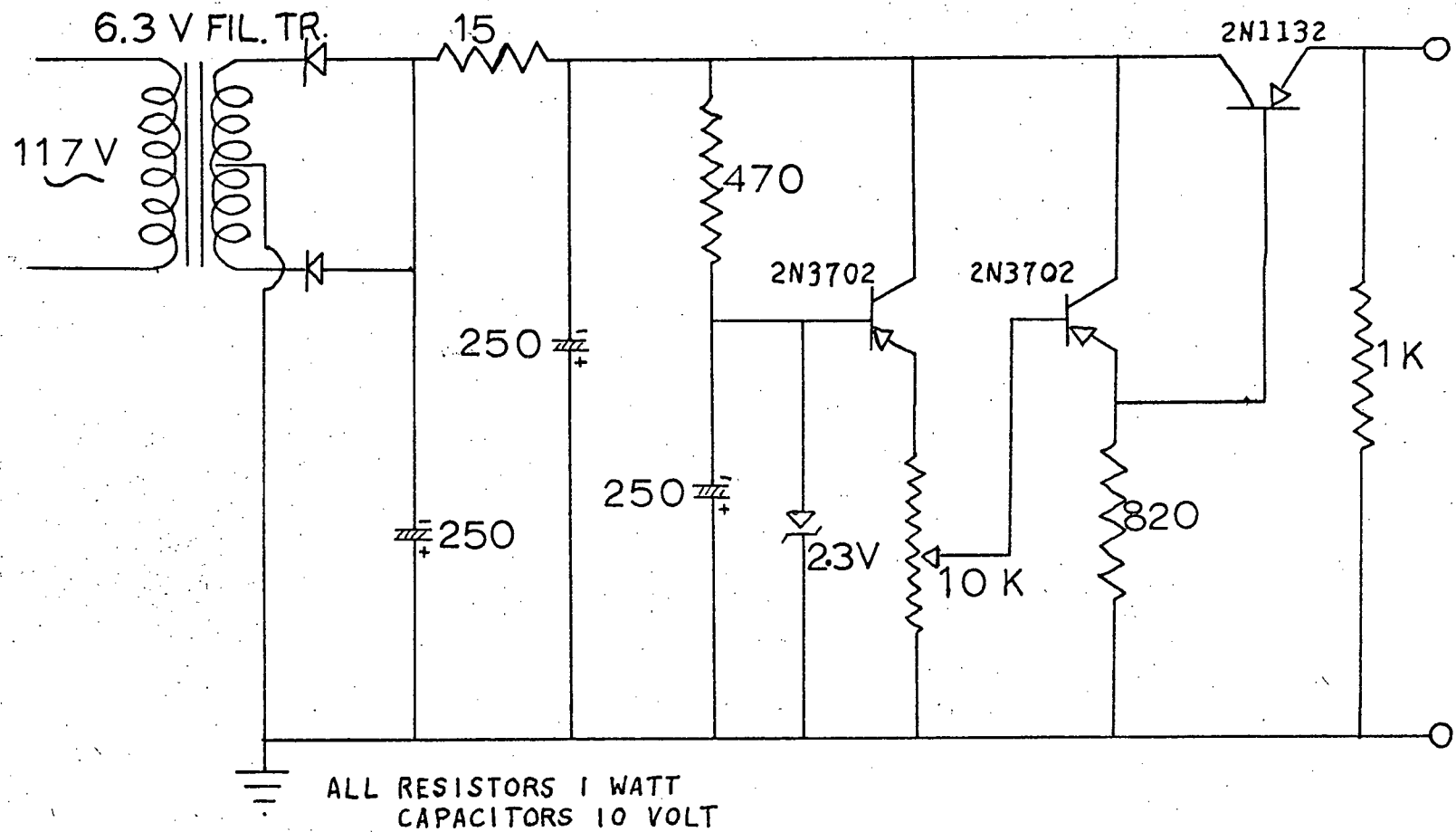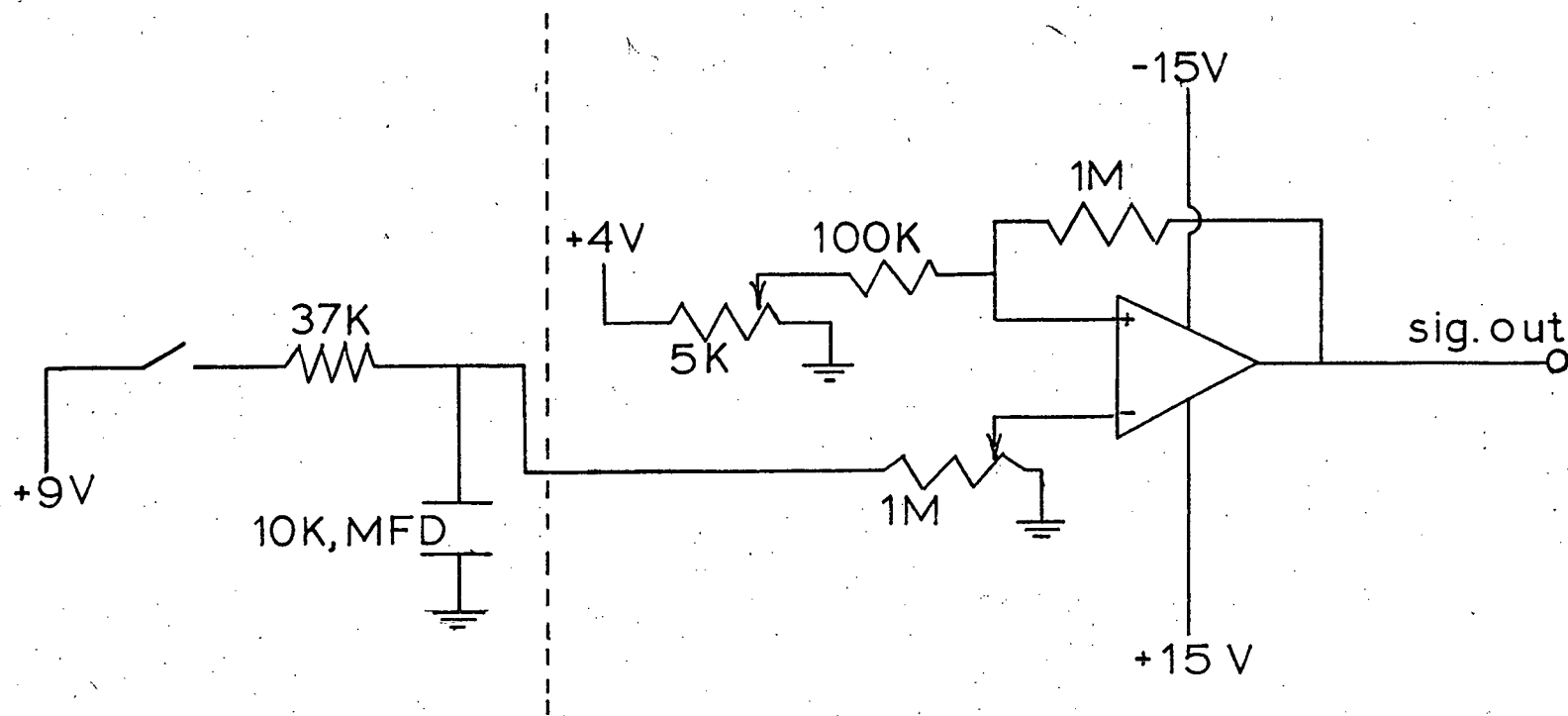
FIG. 11--Helmholtz Coil Power Supply

FIG. 12--Pre-Amplifier and R.C. Circuit

magnetic field to within 0.5% of the known value. Since the specifica-
tions for the gaussmeter stipulated that its scale could be changed with
an error of less than 1.5%, this gaussmeter was believed to be accurate
to 2%. In order to save calibrating the x-channel of the x-y recorder,
the position of the pen was measured as a function of the field. With
the recorder on the 2 V/in. scale, (which was always used in its
calibration mode), the field in the discharge region was found to be
3.90 ± .08 gauss per inch of the pen movement.

The direction of observation which was also the direction of the
applied magnetic field was align with the horizontal component of the
earth's magnetic field. With this orientation the earth's magnetic
field was cancelled by the applied magnetic field.

The vertical component of the earth's magnetic field is cancelled
by a set of smaller Helmholtz coils which were placed inside the pre-
viously mentioned ones. These coils can be made smaller with the same
absolute homogeneity in magnetic fields because one is dealing with a
smaller magnetic field. These coils are 19.5 cm in diameter and 9.7 cm
apart. Each coil has 50 turns of #24 copper wire.

The current for the above coils is provided by a small power supply
delivering up to 1 V and 150 ma. Thus, when the 2 coils are placed in
series the field produced at the centre can reach approximately .7
guass. Since the object of these coils was to make the vertical component,
(y-axis), of the magnetic field zero, the calibration, of sorts, was
done with a dip needle. That is, the dip needle was placed in the position
of the discharge cell, and the current was adjusted until the dip needle
read zero magnetic field. Fields down to approximately .01 gauss could

be measured this way.

3.9   Photomultiplier

The photomultiplier is an E.M.I. 9558QB with an S-20, (NaKSbCs),

surface and a quantum efficiency of $\simeq 20\%$.   It was operated with a cathode

to anode potential of -1280 V.   The dynode chain resistors were all

33KΩ .   The anode is connected to ground by a 100KΩ resistor.   The

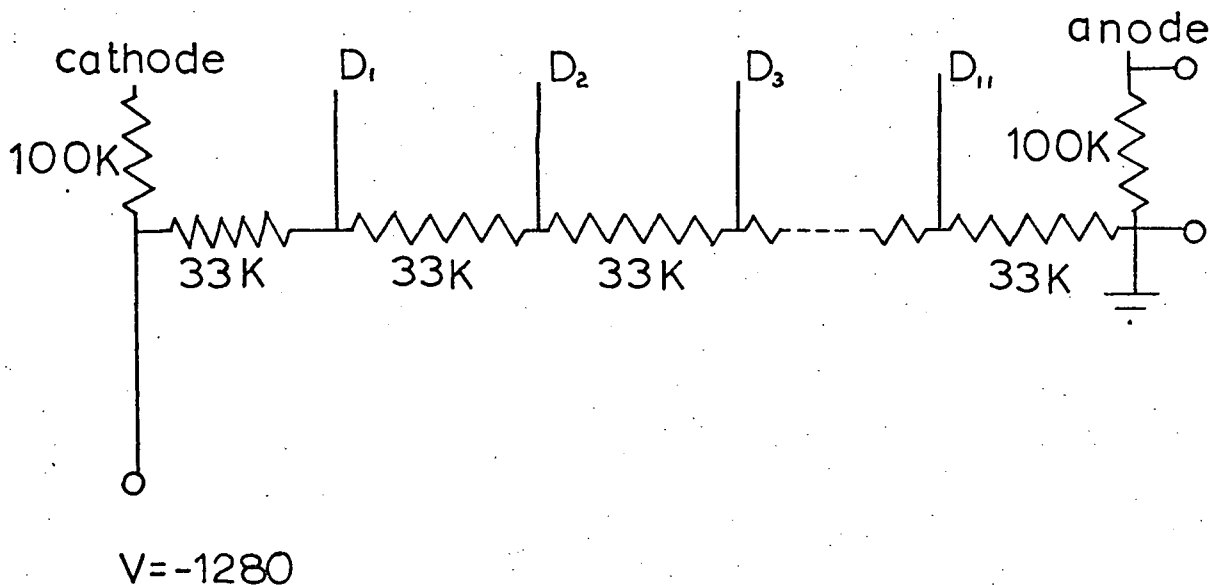abbreviated circuit is shown below in Fig. 13.

FIG. 13--Photomultiplier Wiring System

3.10   X-Y Recorder

The x-y recorder used was a Varian model F100 having a linearity

of 1% and input impendance of 100K Ω into each channel.

3.11   Data Processing

When running the experiment the phase angle ϕ was difficult to set

accurately to zero.   Also, the polarization signal was not noise-free.

Thus, to obtain a more accurate value of the halfwidth, $H_{\frac{1}{2}}$, the graphs plotted by the x-y recorder were subject to numerical processing.

Relative values of the polarization were read from the graphs at 0.2 inch intervals to provide 33 data points. The points were then fitted by a function of the form:

$$ P = C_1 + \frac{C_2}{1 + \frac{1}{H_{\frac{1}{2}}^2} (H - H_o)^2} \left[\cos 2\theta - \frac{1}{H_{\frac{1}{2}}} (H - H_o) \sin 2\theta \right] $$

where C_1, C_2, $H_{\frac{1}{2}}$, H_o, and θ are parameters fitted by a computer "least" squares" fitting routine, (U.B.C. L.Q.F.). From these fitted curves, the $H_{\frac{1}{2}}$ for about 7 different pressures between 0.050 and 0.300 mm Hg were obtained for each transition. These values of $H_{\frac{1}{2}}$ were plotted as a function of pressure and extrapolated to zero pressure. From these extrapolated values the radiative lifetimes of the 3^1D, 4^1D, and 5^1D levels were obtained.

3.12 Special Optical System

For the $3^1D - 2^1P$ spectral line at 6678Å, it was found that, by scanning the spectrum, there were no neighbouring lines between 6100Å and 7010Å. Thus, it was possible to replace the monochromator by an Optics Technology Inc. interference filter; set no. 3099, filter no. 666 (see Fig. 14). The specifications on this filter indicated a pass-band of 6700Å $\pm$ 200Å. A line which showed up at 7010Å had no appreciable effect when viewed through the filter. Since this filter had no polarizing effects, it was possible to measure the absolute amount of polarization, and the steadiness of the overall signal as the magnetic field was swept. To measure the percentage of polarization as a function of

filter   polaroid   rotating
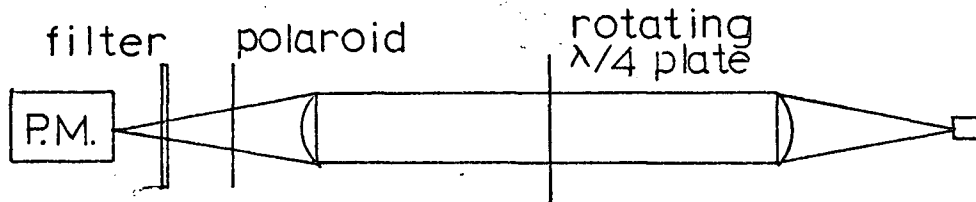   λ/4 plate
P.M.

FIG. 14--Special Optical System.

the magnetic field, the rotating quarter-wave plate was removed. The

light was transmitted, in turn, through a polaroid, the filter, and

then into the photomultiplier. The signal from the photomultiplier was

then fed directly into the x-y recorder, bypassing the phase sensitive

detector. This procedure was repeated, except with the polaroid removed,

to measure how the entire signal varied with the magnetic field strength.

This method was used only to measure the polarization and stability of

the light emitted from the discharge. The previous optical system was

used to measure the lifetime of the 3^1D state of helium.

CHAPTER IV

RESULTS

4.1   Lifetimes

In this experiment the lifetimes of three energy levels were measured. As mentioned previously they were the 3D, 4D, and 5D singlet states of the helium atom. In Fig. 15 is shown a typical experimental plot of the 4^1D polarization curve. In Fig. 16 is its "least squares" fitted curve.

The halfwidth, $H_{\frac{1}{2}}$, was measured for Hanle signals at several pressures. Graphs of $H_{\frac{1}{2}}$ plotted as a function of pressure are shown in Figs. 17, 18 and 19 for the 5^1D, 4^1D and 3^1D levels respectively. The halfwidth of a line at zero pressure was obtained by extrapolation. The upper state lifetimes,   , were computed from the following equation:

$$\tau = \frac{\hbar}{2\mu_o g H_{\frac{1}{2}}}$$

The lifetimes obtained for these levels are listed in Table II, III, and IV along with their respective lifetimes obtained by various other workers.

Besides the three states mentioned above, the 6^1D, 7^1D, 8^1D and 9^1D states were attempted through the transitions $n^1D - 2^1P$. But the signal to noise ratio was so small for these transitions, that no worthwhile data was recorded.

4.2   Cross-sections

The lifetime of a certain level is shortened as a result of collisions of an atom with its neighbour. The number of collisions per second
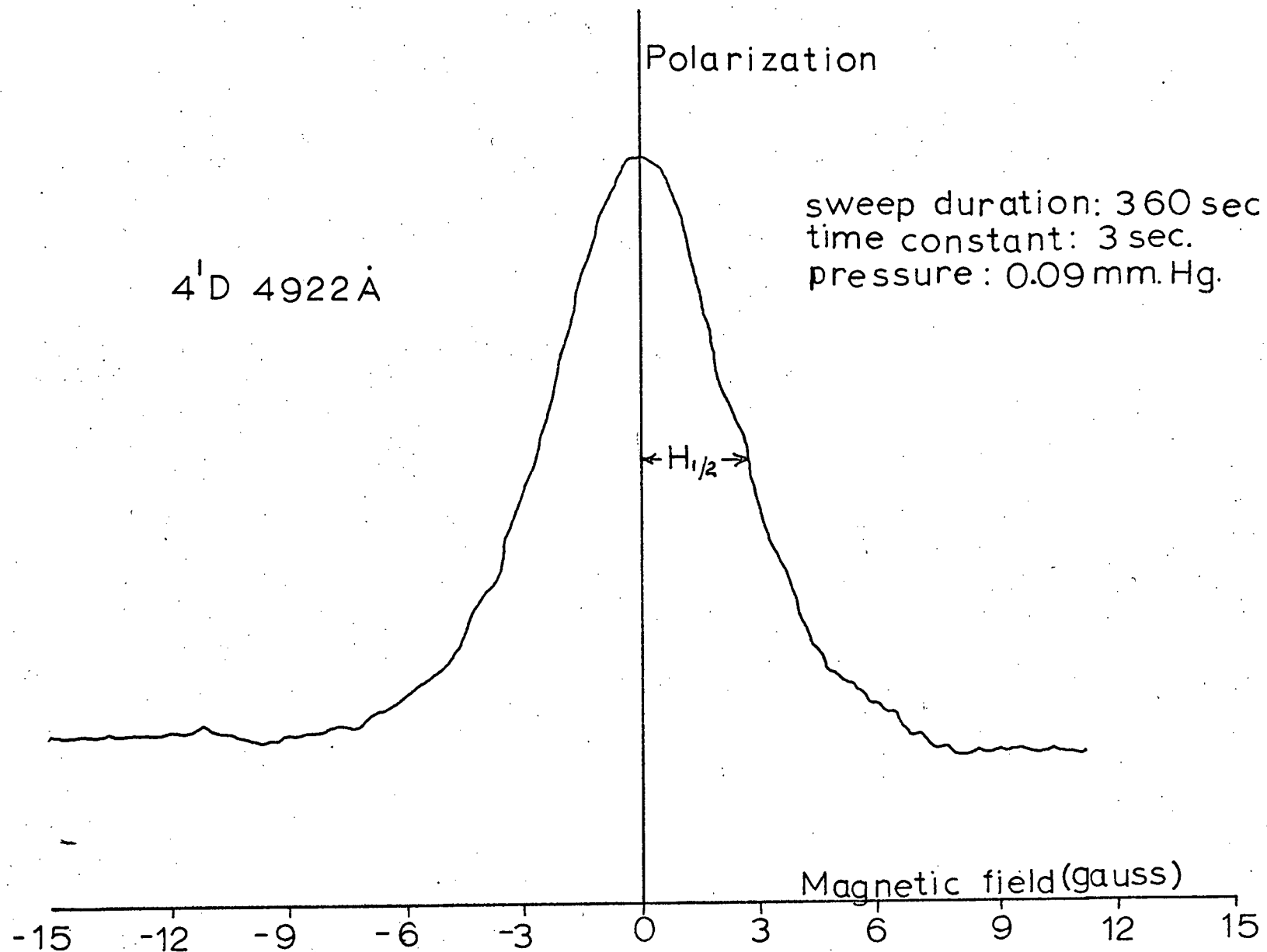
FIG. 15--Experimental Level-Crossing Curve for the 4^1D Line

POLARIZATION

4'D – 2'P
PRESSURE: .090 mm Hg

MAGNETIC FIELD

-10.0 -8.0 -6.0 -4.0 -2.0 0.0 2.0 4.0 6.0 8.0 10.0 GAUSS
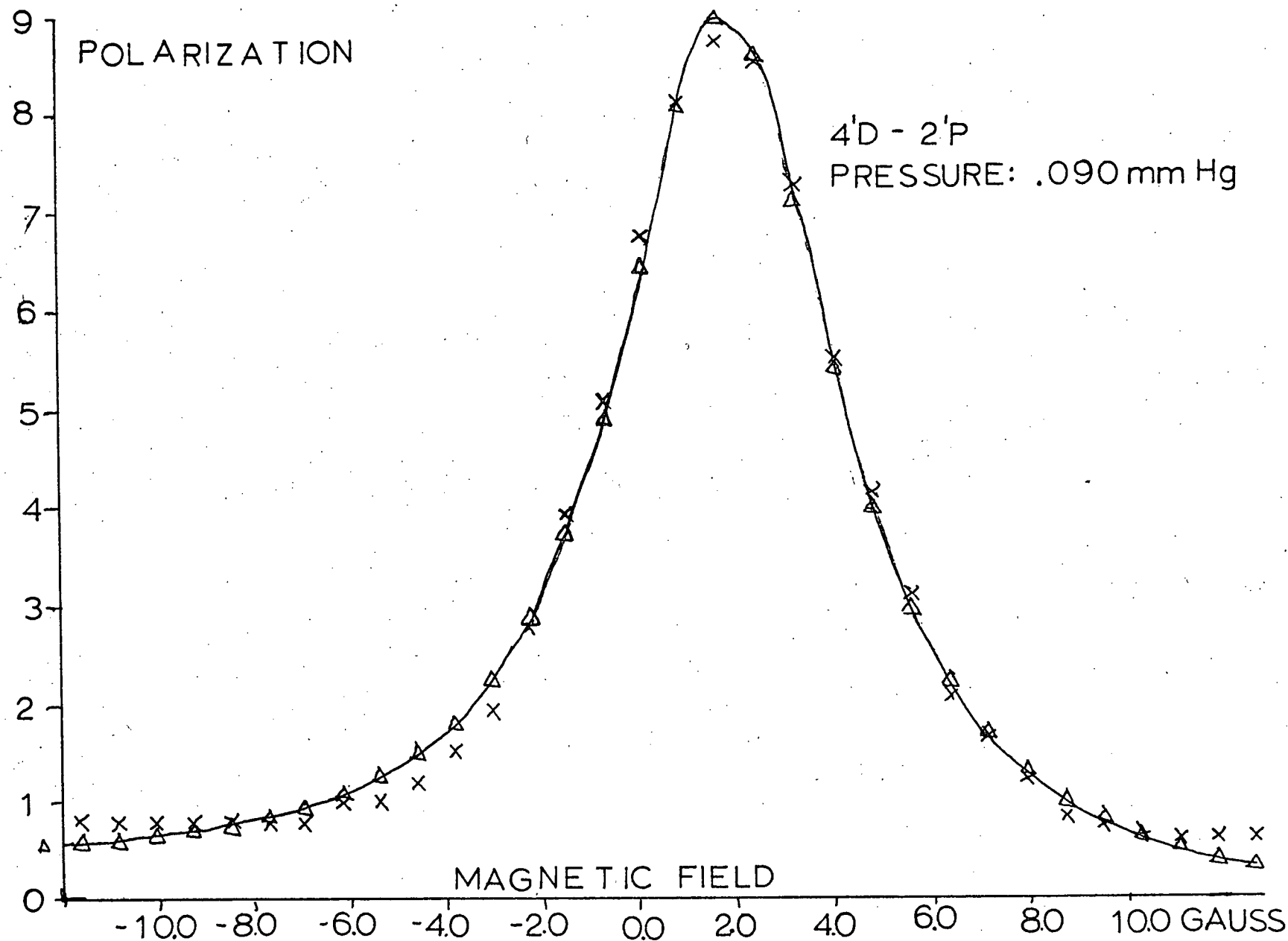
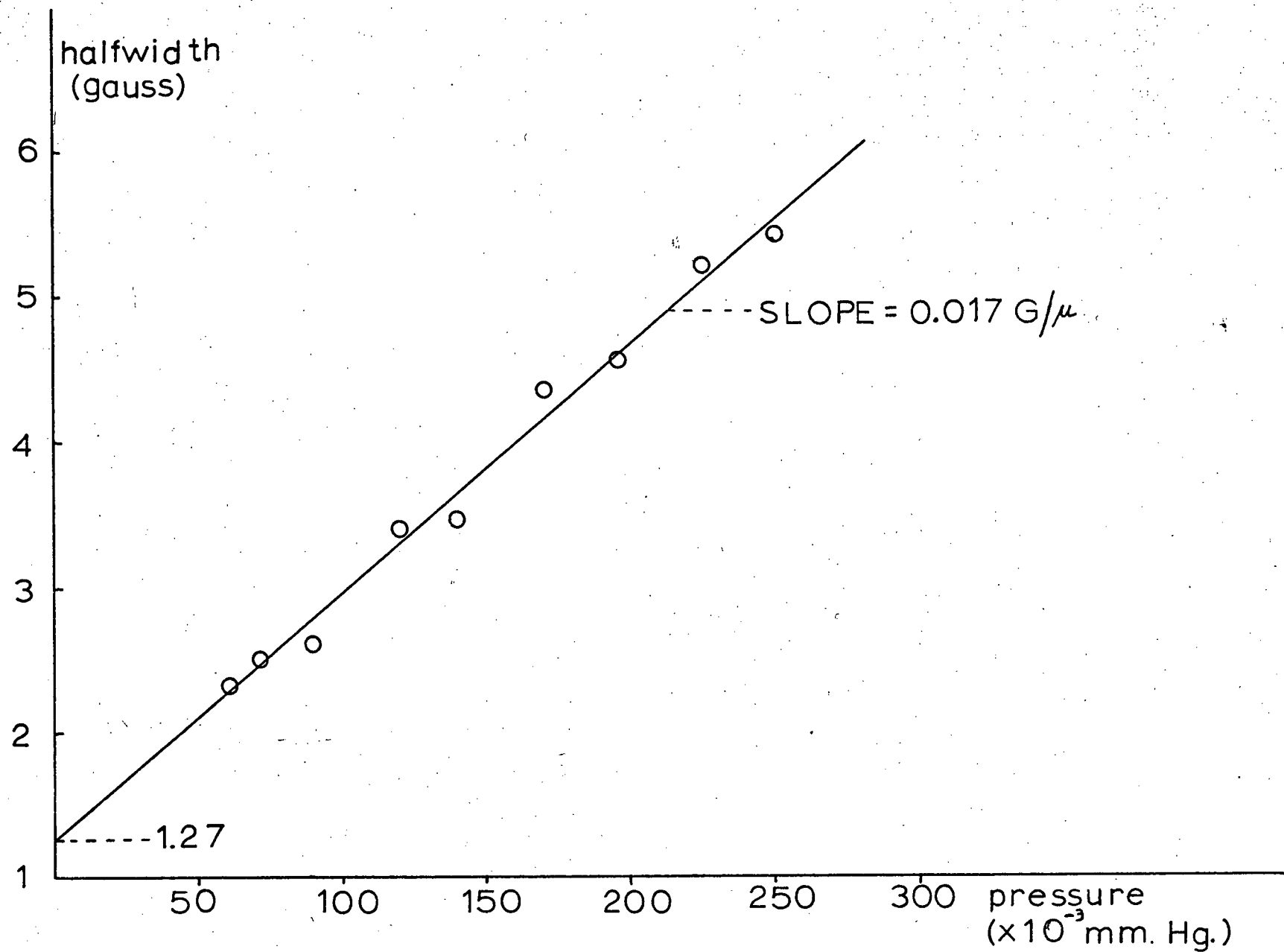FIG. 16--Least Squares Fitted Curve for the 4^1D Line

FIG. 17--Plot of $H_{\frac{1}{2}}$ as a Function of Pressure of 5^1D State
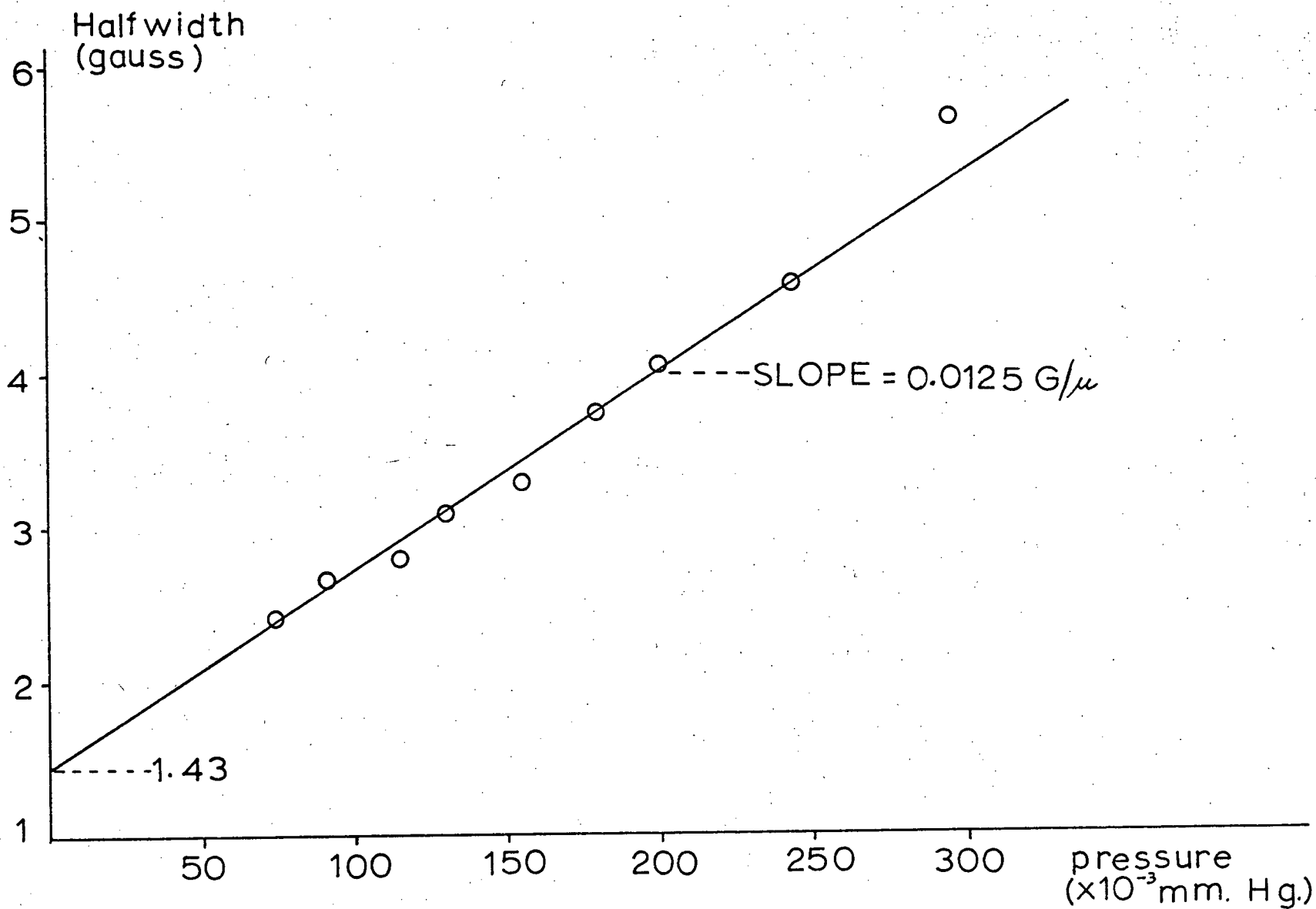
FIG. 18--Plot of $H_{\frac{1}{2}}$ as a Function of Pressure of 4^1D State
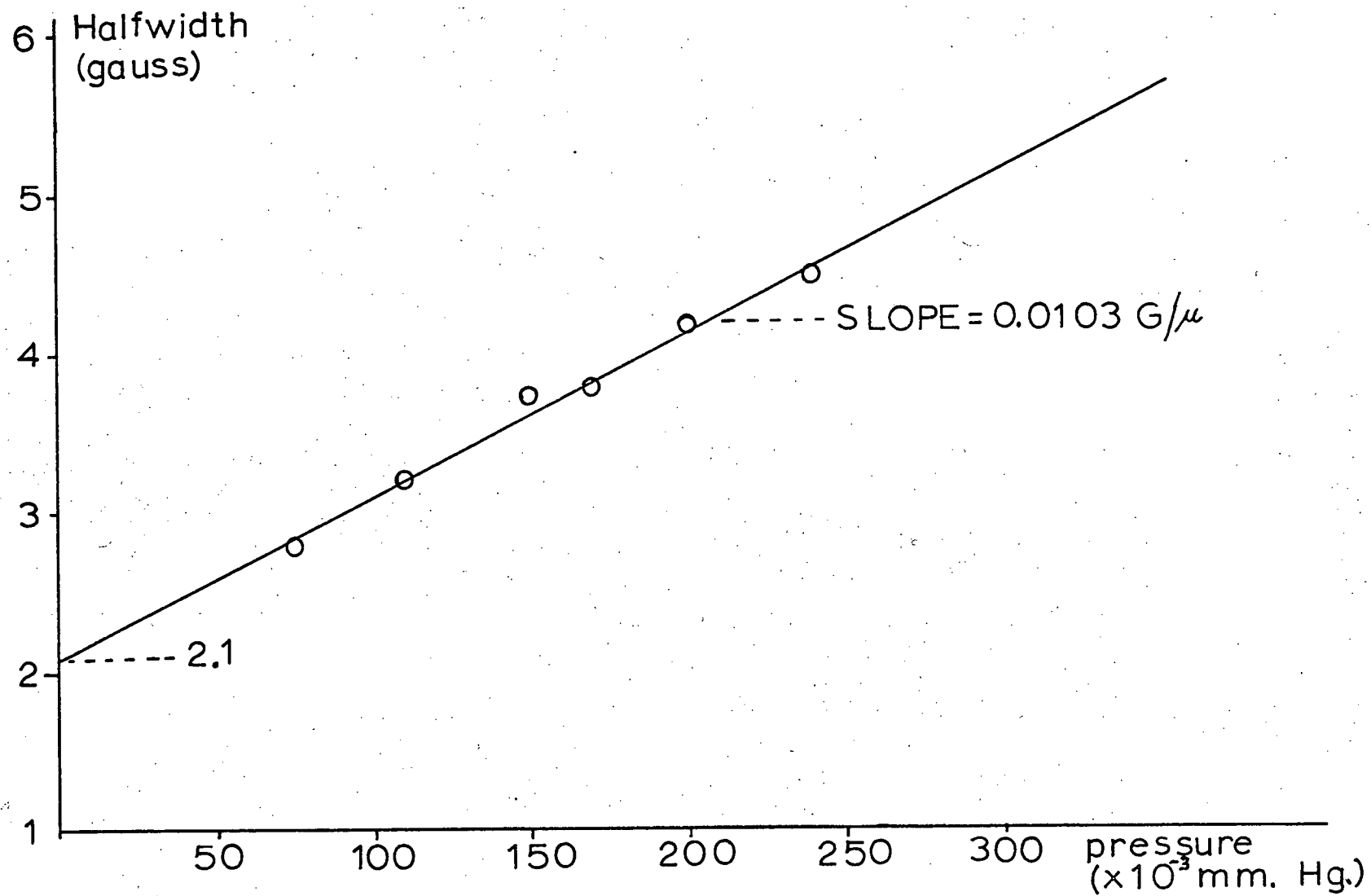
FIG. 19--Plot of $H_{\frac{1}{2}}$ as a Function of Pressure of the 3^1D State

TABLE II.--LIFETIME OF THE 5^1D STATE OF HELIUM

$(x10^{-8}sec)$	Author	Technique	Date
6.6 ±.4	I. Martison et al.[15]	Beam foil	1969
4.91±.2	Descomps et al.[14]	Magnetic Resonance	1960
4.9 ±.5	J. P. Descoubes[13]	Level Crossing	1967
7.9 ±.6	Pendleton & Hughes[8]	Direct observation of decay	1965
4.6 ±.3	Kindleman & Bennett[9]	Delayed coincidence	1963
6.3 ±.9	Bridgett & King[10]	Direct observation of decay	1967
4.6 ±.3	Osherovich & Verolaimen[11]	Delayed coincidence	1968
7.16	Wiese et al.[12]	Theoretical	1965
4.48±.4	Ours	Level Crossing	

TABLE III.--LIFETIME OF THE 4^1D STATE OF HELIUM

($\times 10^{-8}$ sec)	Author	Technique	Date
3.8 ±.3	I. Martison et al.[15]	Beam foil	1969
3.91±.2	Descomps et al.[14]	Magnetic Resonance	1960
4.1 ±.5	J. P. Descoubes[13]	Level Crossing	1967
4.7 ±.5	Pendleton & Hughes[8]	Direct observation of decay	1965
3.0 ±.5	Kindleman & Bennett[9]	Delayed coincidence	1963
3.5 ±.4	Fowler et al.[16]	Direct observation of decay	1964
3.9 ±.5	Bridgett & King[10]	Direct observation of decay	1967
3.8 ±.5	Allen et al.[17]	Direct observation of decay	1969
3.66	Wiese et al.[12]	Theoretical	1965
3.97±.4	Ours	Level Crossing	

TABLE IV--LIFETIME OF THE 3^1D STATE OF HELIUM

| ($\times 10^{-8}$ sec) Author	Technique	Date
1.2 ±.3 J. P. Descoubes[13]	Level Crossing	1967
1.6 ±.2 Pendleton & Hughes[8]	Direct observation of decay	1965
1.6 ±.4 Kindleman & Bennett[9]	Delayed coincidence	1963
1.8 ±.5 Fowler et al.[16]	Direct observation of decay	1964
1.55 ±.5 Allen et al.[17]	Direct observation of decay	1969
1.6 ±.1 Osherovich & Verolaimen[11]	Delayed coincidence	1968
1.5 Wiese et al.[12]	Theoretical	1965
2.71 ±.3 Ours	Level Crossing	
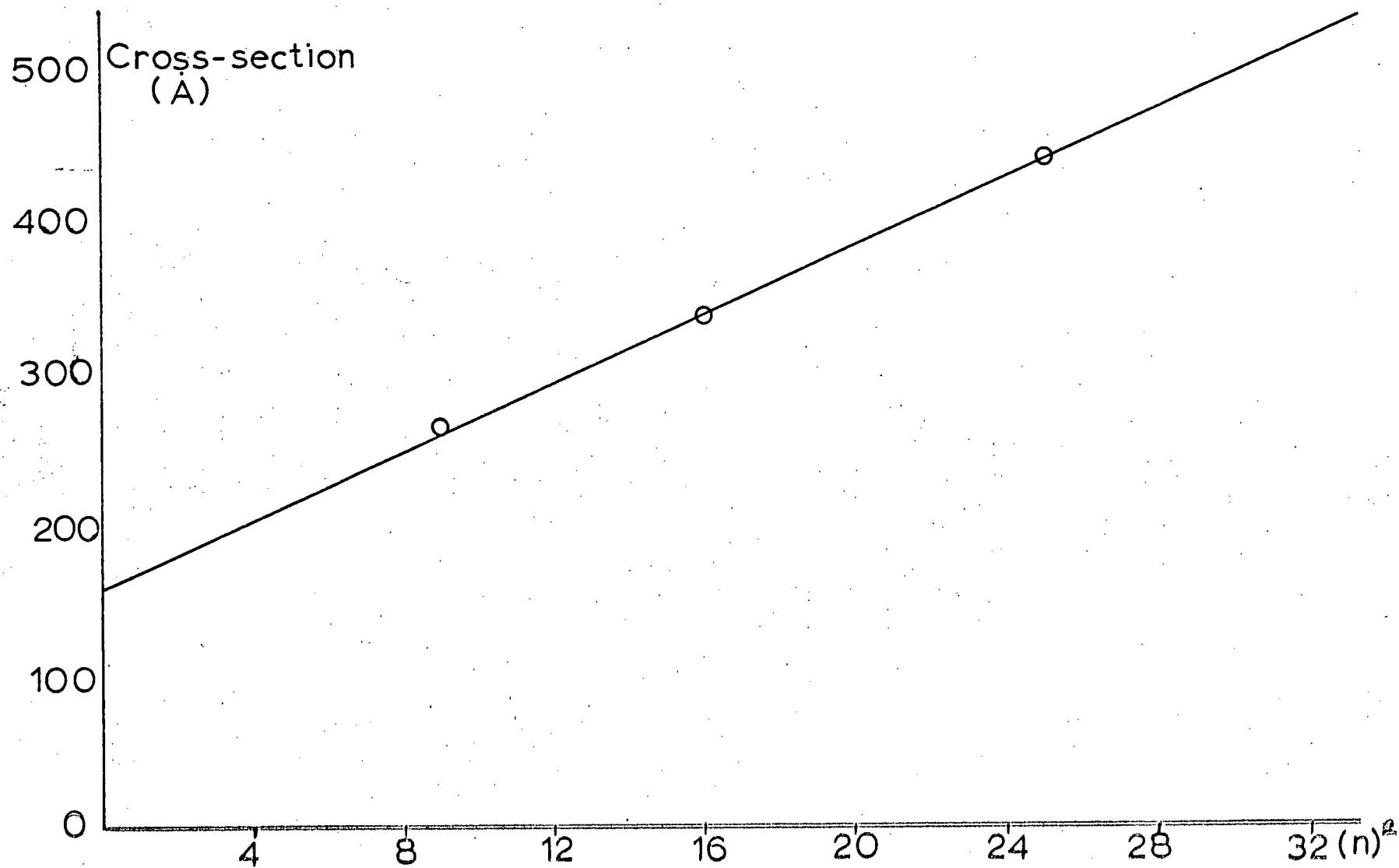
FIG. 20--Plot of Cross-Sections as a Function of n^2

is proportional to the pressure. Therefore, from the slope of the $H_{\frac{1}{2}}$ versus pressure graphs in Figs. 17, 18 and 19, one can calculate reasonable values for the cross-sections of the helium atom in various energy levels. From Appendix 2 the cross-section, , is:

$$\sigma = \frac{1}{\rho \, \nu \, L} \text{ (slope of } H_{\frac{1}{2}} \text{ curve) } (2.59 \times 10^{-12}) cm^2$$

where ν is the mean velocity of the atoms (assume that σ is independent of σ) and   is the density of the atoms at a pressure, P_2, which is the pressure it would take to divide the lifetime in half. The cross-sections of the helium atom in the 3^1D, 4^1D, and 5^1D states are listed in Table V and plotted as a function of the square of the quantum number n in Fig. 20.

TABLE V.--CROSS-SECTIONS

Atomic State n	Cross-section
3^1D	266 Å
4^1D	366 Å
5^1D	440 Å

4.3 Stability and Polarization of the Discharge

It was important to know if the amplitude of the signal from the discharge varied with the magnetic field. This was tested by looking at the 3^1D - 2^1P transition as discussed in Section 3.12 (i.e. using an interference filter instead of the monochrometer). Below is shown a trace from the x-y recorder, of the amplitude of the emitted light as a function of the magnetic field (Fig. 21). As we assumed in the theory, it was unaffected by the magnetic field to within 1%.

Another interesting feature was investigated. This was the percentage of polarization of the signal.   Again,   this was done by observing
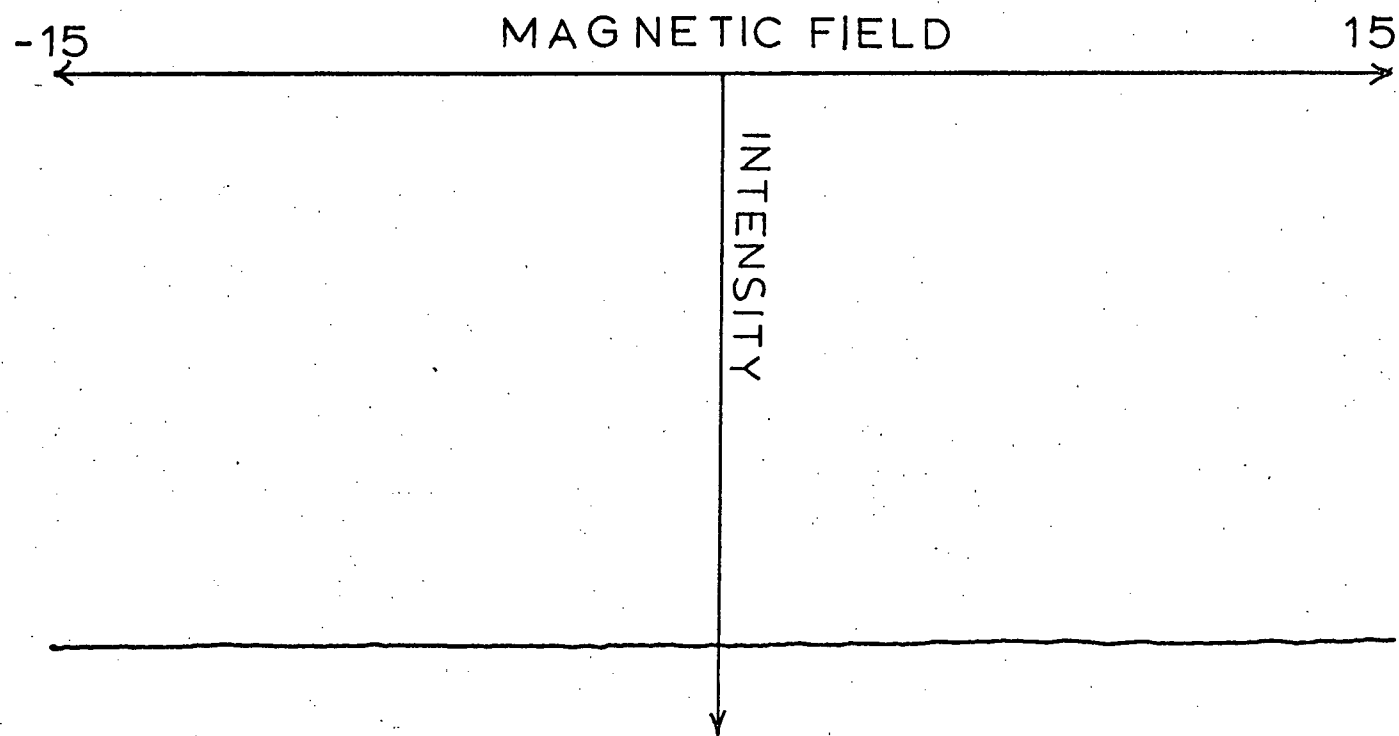
MAGNETIC FIELD

-15

15

INTENSITY

FIG. 21--Plot of Intensity as a Function of Magnetic Field

MAGNETIC FIELD

-15 G

+15 G.
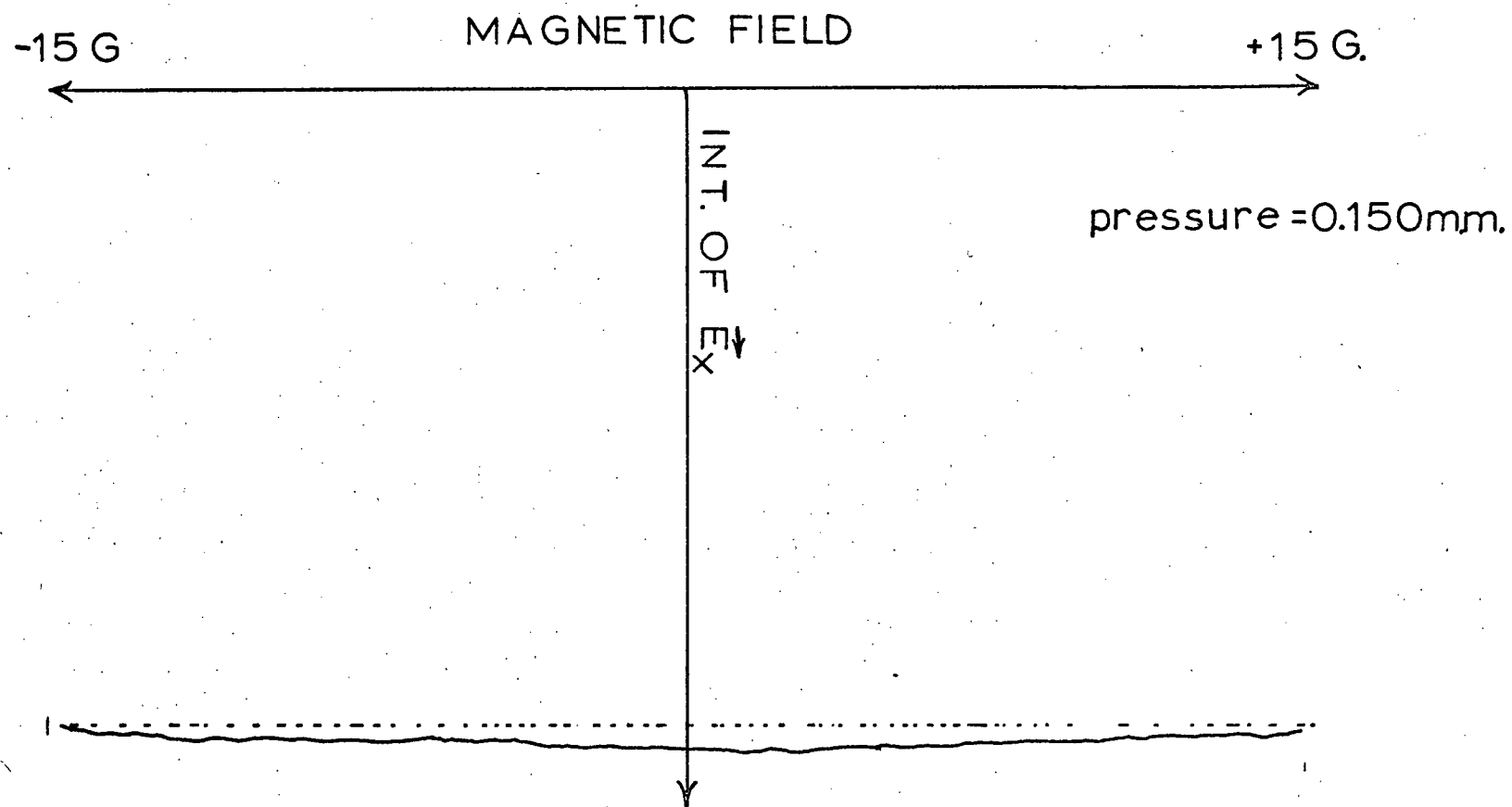
INT. OF Ex↓

pressure=0.150mm.

FIG. 22--Polarization Plotted as a Function of Magnetic Field

the $3^1D - 2^1P$ transition line through an interference filter. As one can see from Fig. 22, at a pressure of .095 mm Hg, the polarization is about 3%, using the phase sensitive detection system we were able to obtain a large signal to noise ratio for pressures between .060 mm Hg and .250 mm Hg.

The minimum pressure of helium at which the discharge would continually run was .060 mm Hg. At .050 mm Hg the discharge could be started with a Tesla coil, but the intensity would decrease to zero within 30 seconds. I assumed that the electron source was helium atoms. Thus at lower pressures the discharge did not function because of too low a density of electrons. The above mentioned use of the Tesla coil strengthens this argument.

At .060 mm Hg the discharge would run proficiently only when the stopcock to the McLeod gauge was left open. (It was assumed that mercury vapour was present.) Within about 3 minutes after this stopcock was closed, the amplitude of the intensity and polarization of the light signal decreased by a factor of 5. Also, the width of the curve became broader. Below, in Fig. 23, are shown two polarization curves; one with the stopcock opened and mercury vapour present and the other with no mercury present. Both have a total pressure of .060 mm Hg. This change in intensity can be explained by a change in the electron density. Since the ionization energy of mercury is less than helium, a discharge of a mixture of mercury and helium at .060 mm Hg will have a higher density of free electrons than a discharge of pure helium.

The discrepancy of $H_{\frac{1}{2}}$ in Fig. 23 could have been caused by an unstable discharge. At .060 mm Hg of pure helium the discharge is more or less at its excitation threshold (i.e. unstable). Thus the magnetic
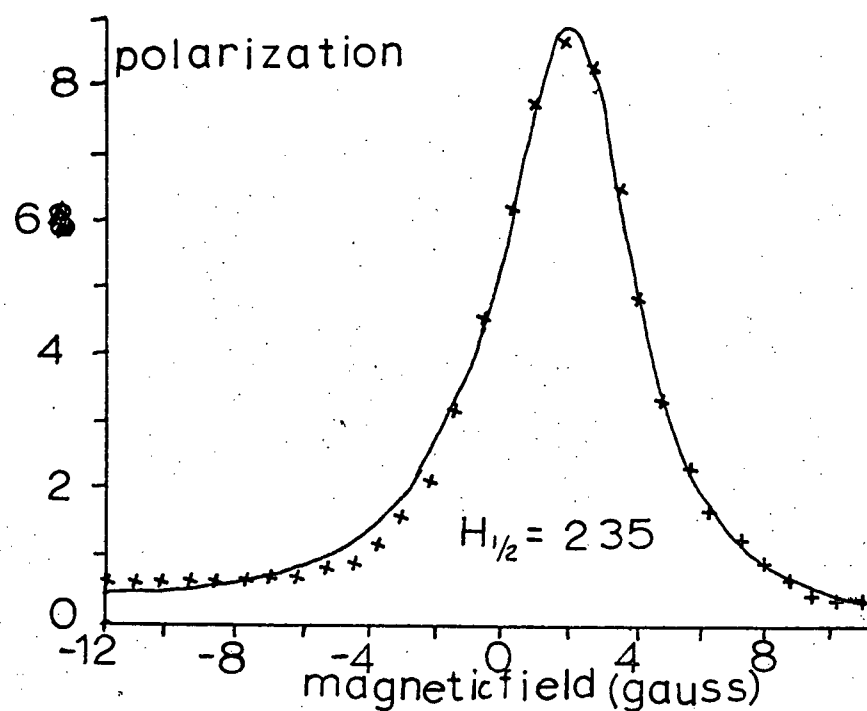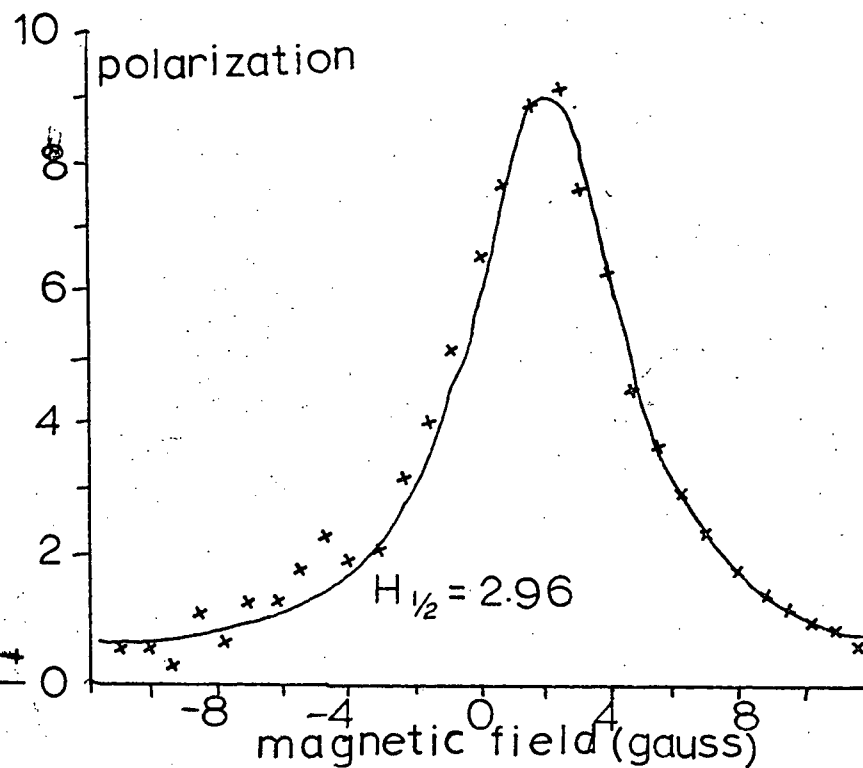
FIG. 23--Fitted Curves of Runs at Low Pressures

field could have had a large effect on the intensity of the emitted light which would have an effect on $H_{\frac{1}{2}}$.

4.4   Experimental Errors

a)   Magnetic Field

The calibration of the magnetic field was done with a gaussmeter that was capable of measuring the magnetic field to an absolute accuracy of 0.2 gauss.

The linearity of the magnetic field calibration could be effected by; ohmic heating of the coils, hysteresis effects in nearby ferro-magnetic materials, and residual earth magnetic fields. To investigate this, the output of the gaussmeter was fed into the y-channel of the x-y recorder and the magnetic field, which was fed into the x-channel, was swept from -15 gauss to +15 gauss. From this recording it was observed that the magnetic field was linear to within 1%.

b)   Pressure in the Discharge

Due to the scale on the McLeod gauge, the accuracy to which the pressure could be measured was 7%. From Fig. 10, it is noted that the pressure in the discharge cell could be different from that in the McLeod gauge. But these pressures are still proportional to each other. Therefore the extrapolated values of $H_{\frac{1}{2}}$ are correct, but the slope of the $H_{\frac{1}{2}}$ versus pressures curves could be out by 20%. This would effect only the calculation of the cross-sections.

c)   Temperature in the Discharge

The temperature of the gas in the discharge affects only the cal-culation of the absolute value of the cross-sections. Since the relative values are unaffected, this error has no effect on the straight line for

the plot of the cross-sections as a function of n^2 in Fig. 20. The temperature of the discharge was assumed to be 300°K, the room temperature. The computed cross-section varies as $T^{\frac{1}{2}}$, thus a $\pm 25^{\circ}$K error in the assumed temperature of the discharge will affect the results by only 4%.

d) R.F. Broadening

The radio frequency electric field, E, of the discharge is about 300 - 400 volts/cm. In general this will broaden the polarization curve. In a weak magnetic field (R.F. frequency $\nu \gg \omega_i - \omega_j$) a Stark term is taken into account and the polarization curve then has the form:

$$P = \frac{P_o}{1 + \tau^2 \left[c^2 E^4 + (\omega_i - \omega_j)^2 \right]}$$

When one compares this expression for P with the one that was derived earlier for P, it becomes apparent that the presence of the Stark polarizing term, $c^2 E^4$, will tend to broaden the polarization curve. In a paper by Lombardi[18] this broadening was reported to be as much as 30% for low energy transitions. A shielding of the radio frequency electric field, E, by free electrons in the discharge could possibly be a reason to disregard broadening due to Stark polarization in this experiment. As mentioned in Section 4.3, there was a broadening of $H_{\frac{1}{2}}$ at low pressures (and hence low electron densities), which would be consistent with the free electron shielding hypothesis. Also the values of $H_{\frac{1}{2}}$ in this experiment are on the whole, narrower than values measured previously by other workers.

CHAPTER V

CONCLUSIONS

The accuracy of this method, as in most experiments, depends on the signal to noise ratio. Before the signal reaches the photomultiplier it must pass through a quarter-wave plate and a monochromator which reduces the entire signal by about 50%. The signal which is being measured, is proportional to the percentage of polarization of the emitted light. As was shown in Section 4.3 this is only about 3%. Therefore, a criterion for performing this experiment is a strong light source.

An improvement which would simplify the experimental procedure and increase the signal to noise ratio would be to replace the monochromator with an interference filter than has no polarizing effects.

Excitation of an atom or molecule by an electron beam permits Hanle effect measurements of most states of atoms which have strong dipole transition to a lower state and possess Zeeman sublevels. An upper limit on the lifetimes that can be measured (how narrow $H_{\frac{1}{2}}$ is in Fig. A), depends on the linearity of the varying magnetic fields and the accuracy of the control of the earth's magnetic field. In this case the upper limit is 10^{-7} sec. The lower limit of lifetimes is affected by the size of the product of $g\tau$. If $g\tau$ is large the polarization curve that fits the equation

$$P = \frac{P_o}{1 + (\mu_o g \tau H_{\frac{1}{2}})^2}$$

will be extremely broad. To measure broad curves a high signal to noise

ratio is required. Thus with the light source used in this experiment a lower limit of 10^{-10} sec is set for the product of $g\tau$.

From the graphs in Figs. 17, 18 and 19, one can see that the experimental values of $H_{\frac{1}{2}}$ plotted as a function of pressure form a convincing straight line.

The straight line agreement of the graph in Fig. 20, which is a plot of the cross-sections as a function of the square of the quantum number, agrees with the classical theory of the atom.

There is good agreement between the values we measured for the lifetimes of the 4^1D and 5^1D states and the values previously found, as can be seen in Tables II and III.

There is a noticeable discrepancy between our results and previous measurements of the lifetime of the 3^1D level. We used the same technique to measure τ , for all three levels, and the extrapolation shown in Fig. 19 seems reasonable. We are unable to suggest why our results and those of previous measurements for the 3^1D level are in such bad agreement.

APPENDIX I

ROTATING QUARTER-WAVE PLATE

The optical system described in Section 3.3 is schematically shown below in Fig. 24.

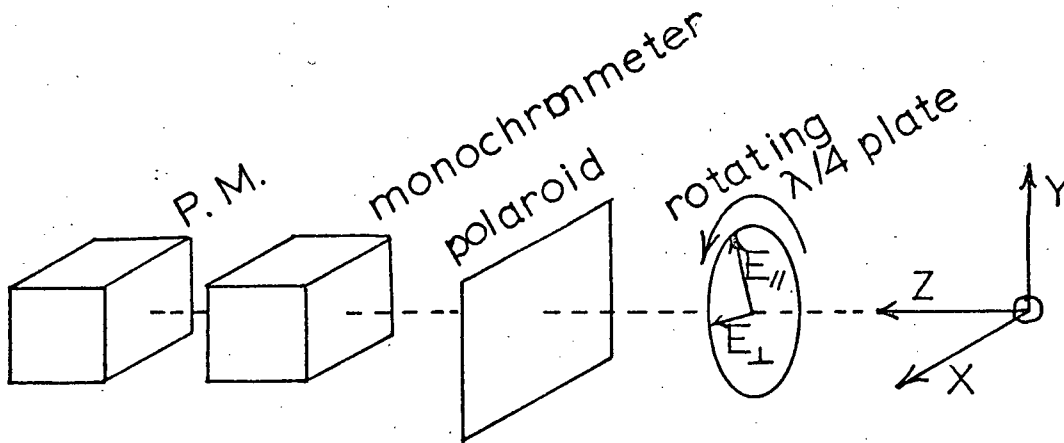FIG. 24--Optical Schematic

A signal, polarized at an angle to x-axis, is transmitted from the discharge cell in the z-direction. The x and y components of the signal are:

$$E_x = A_o \cos\Theta \, \exp\left[\,i(kx - \nu t)\right]$$
$$E_y = A_o \sin\Theta \, \exp\left[\,i(kx - \nu t)\right]$$

(1)

The polarization is defined to be:

$$P = \frac{E_x^2 - E_y^2}{E_x^2 - E_y^2} = \cos^2\Theta - \sin^2\Theta$$

This signal was then passed through the rotating quarter-wave plate. To express the outcome, I set up a rotating coordinate system. It was fixed to the quarter-wave plate, such that $E_{\parallel}$ was parallel to the slow axis and $E_{\perp}$ was perpendicular to the slow axis. This coordinate system was rotating at a frequency ω. The $E_{\parallel}$ and $E_{\perp}$ coordinates, expressed in terms of E_x and E_y, are:

$$E_{\parallel} = E_x \cos(\omega t + \phi) + E_y \sin(\omega t + \phi)$$

$$E_{\perp} = E_y \cos(\omega t + \phi) - E_x \sin(\omega t + \phi)$$

where ϕ is an arbitrary phase angle. Setting $\phi = 0$ and expressing the signal after it had passed through the quarter-wave plate in terms of $E_{\parallel}$ and $E_{\perp}$.

$$E_{\parallel}' = E_{\parallel} \exp(i\delta)$$

$$E_{\perp}' = E_{\perp} \exp\ i(\delta - \pi/4) \quad = - i\ E_{\perp} \exp(i\delta)$$

Transforming into the stationary x-y coordinate system:

$$E_x' = \cos(\omega t) E_{\parallel}' - \sin(\omega t) E_{\perp}'$$

$$E_y' = \sin(\omega t) E_{\parallel}' - \cos(\omega t) E_{\perp}'$$

At this point the signal passes through a polaroid with its axis in the y direction. Now the above signal becomes:

$$E_x'' = 0$$

$$E_y'' = E_y'$$

The polaroid was align with its axis of polarization parallel to the axis of polarization of the monochrometer. Therefore the signal which passed through the monochrometer and reached the photomultiplier was

the same as the input signal to the monochrometer. The signal recorded

by the photomultiplier is proportional to:

$$\left| E_y'' \right|^2 = \left| \sin(\omega t)E_{//} - i \cos(\omega t)E_{\perp} \right|^2 \tag{2}$$

By substituting the above values for $E_{//}$ and $E_{\perp}$ into Equation

(2) and performing some algebraic operations, one gets:

$$\left| E_y'' \right|^2 = \frac{A_o^2}{2} \left\{ -1 + \left[\frac{\cos4 \ + 1}{2} \right] \cos 2\theta - \frac{1}{2} \sin(4\omega t)\sin 2\theta \right\} \tag{3}$$

As is shown in Section 3.4, when this signal is analyzed by the phase

sensitive detector the output signal L is:

$$L \propto \frac{A_o^2 \pi}{16} \left[\cos^2\theta - \sin^2\theta \right]$$

Using the definition of polarization given earlier, it is seen

that the output of the phase sensitive detector is proportional to the

polarization.

APPENDIX II

CROSS-SECTIONS

The following assumptions were made about the discharge:

  i) The number of free electrons in the discharge cell is small

      compared to the number of neutral atoms.

  ii) The number of excited atoms is small compared to the number

      of ground state atoms.

From these assumptions, the lifetime of an excited state of an atom is

shortened by collisions with atoms only in the ground level. If one

considers a plot of $H_{\frac{1}{2}}$ as a function pressure and remember that $H_{\frac{1}{2}} \propto \frac{1}{\tau}$

then the following properties are noted (see Fig. 25).
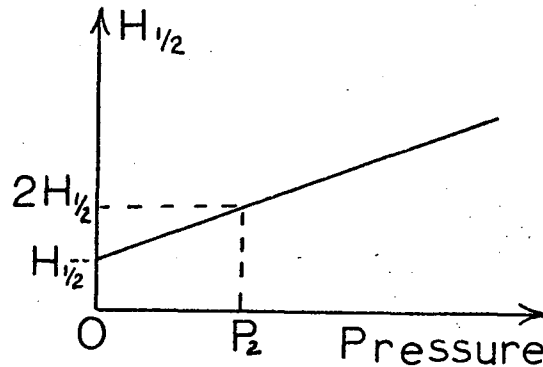

FIG. 25--Sample Cross-Section Plot

When the pressure is zero no transitions are caused by collisions.

At pressure $P = P_2$, τ is $\frac{1}{2}$ of its value when $P = 0$. The number of

transitions per sec., $N^* = \frac{1}{\tau}$ by definition. Therefore, the number of

transitions, N, at $P = P_2$ is twice the number of transitions, N^*, at

P = 0. Half of N is a result of the collision and half is a result of

spontaneous radiation. Therefore, at a pressure $P = P_2$, the number of

collisions is $M = N^* = \dfrac{1}{\tau}$ but $M = \bar{\nu} \rho \sigma$. Therefore, the following

expression can be derived for σ:

$$\sigma = \frac{1}{\bar{\nu} \rho \tau} = (\text{Slope of } H_{\frac{1}{2}} \text{ curve}) \cdot (2.59 \times 10^{-12} \text{cm}^2)$$

where σ is the cross-section, ρ is the density at a pressure of

$P = P_2$, and $\bar{\nu}$ is the mean velocity of atoms.

LIST OF REFERENCES

1   A. C. G. Mitchell and M. W. Zemansky, Resonance Radiation and
    Excited Atoms, pp. 93-153 (London: Cambridge University Press,
    1961).

2   R. L. DeZafra and W. Kirk, Amer. Journal Phys. 35, 573 (1967).

3   W. Hanle Zeits, f. Physik 30, 93 (1924).

4   G. H. Breit, Revs. Modern Phys. 5, 91 (1933).

5   F. D. Colgrove, P. A. Franken, R. R. Lewis and R. H. Sands, Phys.
    Rev. Letters 3, 420 (1959).

6   J. Vanderlinde, unpublished thesis, University of British Columbia.

7   J. Vanderlinde, unpublished thesis, University of British Columbia.

8   W. R. Pendleton and F. H. Hughes, Phys. Rev. 138A, 683 (1965).

9   P. T. Kindleman and W. R. Bennett, Bull. Amer. Phys. Soc. 8, 87
    (1963).

10 K. A. Bridgett and T. A. King, Proc. Phys. Soc. A92, 75 (London,
    1967).

11 Oshervovich and Verolaimen, Opt. Spec. 24, 81 (1968).

12 W. L. Wiese, M. W. Smith and B. M. Glennon, Atomic Transition
    Probabilities, Vol. NSRDS-NBS4 (Washington, D.C.: U. S. Government
    Printing Office, 1966).

13 J. P. Descoubes, Physics of the One- and Two-Electron Atom, loc.
    cit., p. 341.

14 B. Descomps, J. C. Pebay-Peyroula and J. Brossel, Compt. Rend. Acad.
    Sci. 251, 941 (1961).

15 I. Martison, W. S. Bickel, J. Bromander, H. G. Berry, L. Lundin,
    R. Buchta, and I. Bergstrom, J. Opt. Soc. Amer. 60, 352 (1970).

16 R. G. Fowler, T. M. Holzberlein, C. H. Jacobson and S. J. B. Corrigan,
    Proc. Phys. Soc. A84, 539 (London, 1964).

LIST OF REFERENCES (cont'd.)

17   L. Allen, D. G. C. Jones, D. G. Schofield, Jour. Opt. Soc. Amer. <u>59</u>, 842 (1969).

18   M. Lombardi, Compt. Rend. Acad. Science <u>266</u>, 60 (Paris, 1968).